Copy
RM A56D23

C1

RESEARCH MEMORANDUM

THE USE OF AREA SUCTION FOR IMPROVING THE LONGITUDINAL CHARACTERISTICS OF A THIN UNSWEPT WING-FUSELAGE MODEL WITH LEADING- AND TRAILING-EDGE FLAPS

By David G. Koenig

Ames Aeronautical Laboratory
Moffett Field, Calif.

NATIONAL ADVISORY COMMITTEE
FOR AERONAUTICS

WASHINGTON

July 10, 1956

NACA RM A56D23

NATIONAL ADVISORY COMMITTEE FOR AERONAUTICS

RESEARCH MEMORANDUM

THE USE OF AREA SUCTION FOR IMPROVING THE LONGITUDINAL CHARACTERISTICS OF A THIN UNSWEPT WING-FUSELAGE MODEL WITH LEADING- AND TRAILING-EDGE FLAPS

By David G. Koenig

SUMMARY

An investigation was conducted to determine the effect of porous area suction applied to the knees of full-span leading-edge and part-span trailing-edge flaps installed on an unswept-wing airplane model. The wing was of aspect ratio 3 and had a modified double-wedge section with a thickness of 4.2-percent chord. For a brief test, an unswept horizontal tail was installed on the model 0.62 semispan above the extended wing-chord plane. Most of the tests were made at a Reynolds number of 9.4×10^6 and a Mach number of 0.11.

At an angle of attack of 0°, application of area suction to the trailing-edge flap approximately doubled the trailing-edge-flap lift increment. The suction flow requirements of the trailing-edge flap were close to predictions based on data obtained with a 35° swept-wing model. For angles of attack above 0°, leading-edge flap deflection was required to limit leading-edge flow separation which appeared on the undeflected leading edge and which caused loss in trailing-edge-flap lift increment. For the model with the tail off, the use of boundary-layer control on the trailing-edge flap increased destabilizing pitching-moment changes. However, installation of a horizontal tail markedly reduced these adverse pitching moments.

INTRODUCTION

Designers of supersonic fighter-type aircraft considering the use of thin unswept wings of low aspect ratio are faced with the problem of choosing effective high-lift devices for use at landing and take-off. Wind-tunnel tests made at low speed on small-scale models equipped with

thin unswept wings are reported in references 1 and 2. In these investigations, results were obtained using plain, slotted, or split trailing-edge flaps combined with plain or slotted leading-edge flaps. However, design studies have shown that it would be desirable to obtain greater lift coefficients than were obtained with these types of wing flaps.

It has been found that boundary-layer control by porous area suction can be an effective means of improving lift effectiveness of the trailing-edge flaps as well as improving the effectiveness of a leading-edge flap in delaying leading-edge separation. Area suction was successfully applied to the flap of a 35° swept-wing model in the investigation reported on in references 3 and 4.

In order to study the effectiveness of porous area suction applied to leading- and trailing-edge flaps of a thin unswept wing, the investigation reported herein was undertaken in the 40- by 80-foot wind tunnel. The wing of the model was similar to that of the small-scale models of references 1 and 2, having an aspect ratio of 3 with the three-quarter chord line unswept. The wing had sharp leading edges and was equipped with full-span leading-edge flaps and part-span trailing-edge flaps. The objective of the investigation was the evaluation of the use of area suction on both the leading- and trailing-edge flaps; on the trailing-edge flaps to increase lift coefficient at low wing angles of attack, and on the leading-edge flaps to allow greater leading-edge-flap deflection without flow separation at the knee of the flap, thus maintaining trailing-edge flap effectiveness at higher angles of attack.

NOTATION

a turning angle around knee of flap, deg (see fig. 3)

b wing span, ft

c wing chord, ft

c_t horizontal-tail chord

$\bar{c}$ mean aerodynamic chord, $\frac{2}{S}\int_0^{b/2} c^2 dy$, ft

C_D drag coefficient, $\frac{\text{drag}}{q_\infty S}$

C_L lift coefficient, $\frac{\text{lift}}{q_\infty S}$

ΔC_L lift increment due to trailing-edge flap

C_m pitching-moment coefficient, computed about the quarter-chord point the mean aerodynamic chord, $\frac{\text{pitching moment}}{q_\infty \bar{c} S}$

C_Q flow coefficient, $\frac{Q}{V_\infty S}$

l_t distance from $\frac{\bar{c}}{4}$ to hinge line of horizontal tail, ft

p_∞ free-stream static pressure, lb/sq ft

p wing surface static pressure, lb/sq ft

p_p plenum-chamber static pressure, lb/sq ft

Δp pressure differential across porous material, lb/sq ft

P wing-surface pressure coefficient, $\frac{p - p_\infty}{q_\infty}$

P_p plenum-chamber pressure coefficient, $\frac{p_p - p_\infty}{q_\infty}$

q_∞ free-stream dynamic pressure, lb/sq ft

Q quantity of air removed through porous surface based on standard density, cu ft/sec

R Reynolds number, $\frac{V_\infty \bar{c}}{\nu}$

s distance along airfoil surface from reference line to aft edge of porous opening (see fig. 3), in.

S wing area, sq ft

S_f flap area, sq ft

S_R wing area spanned by flap, sq ft

V_∞ free-stream velocity, ft/sec

w_o suction inflow velocity, ft/sec

x distance along airfoil chord, ft

y spanwise distance from plane of symmetry, ft

z vertical distance of horizontal tail above the extended wing chord plane, ft

α angle of attack of wing-chord plane, deg

δ flap deflection in plane normal to hinge line, deg

δ_e deflection of split elevator flap, deg

η spanwise coordinate, $\frac{2y}{b}$

ν kinematic viscosity, ft^2/sec

Λ sweep angle of flap hinge line, deg

Subscripts

c critical

n leading-edge flap

f trailing-edge flap

I inboard

O outboard

T tunnel-wall correction

MODEL AND APPARATUS

A photograph of the model as mounted in the 40- by 80-foot wind tunnel is shown in figure 1 and the geometric characteristics of the model are presented in figure 2. The wing was of aspect ratio 3.0 and taper ratio 0.4 with the three-quarter chord line unswept. The wing section was a symmetrical double-wedge section modified by rounding the ridge line. The wing was combined with a long slender fuselage which was somewhat underslung with respect to the wing. For limited tests, an unswept horizontal tail of aspect ratio 4 was mounted at a position 62-percent wing semispan above the extended wing-chord plane and at an incidence of -2°. The size and location of the horizontal tail with respect to the wing was as follows: $l_t/\bar{c} = 1.79$, $Z/(b/2) = 0.62$, $S_t/S = 0.20$. To trim the model a split elevator flap was installed on the upper surface of the tail. The flap chord was 25-percent that of the tail chord and extended over the complete tail span.

Both leading- and trailing-edge flaps were hinged near the lower surface with the hinge lines located on the 15- and 71-percent chord lines,

respectively. The trailing-edge flap extended from the fuselage to the 75-percent semispan station; the leading-edge flap extended over the full exposed wing span; and the flap-fuselage gaps for both flaps were sealed for all flap deflections. Porous area suction was applied over the knees of the deflected flaps.

For a brief test, short turning vanes were installed on the fuselage near the knee of the trailing-edge flaps. Details of these vanes are shown in figure 2(c).

A drawing of the flap cross section in the vicinity of the hinge line of the flap is presented in figures 3(a) and 3(b). The porous surface was a perforated metal sheet backed by wool felt and a coarse wire mesh. The metal sheet was 0.008 inch thick, had 4225 holes per square inch, and was 11-percent porous. Two felt porosities were used in the investigation, hereinafter to be referred to as grades 1 and 2 for the more porous and less porous felts, respectively. For the leading-edge flap, grade 2 felt was used with the chordwise thickness variation shown in figure 3(c). For the trailing-edge flaps, both grades 1 and 2 felt were used with chordwise thickness variations shown in figure 3(d). The porosities of the two grades of felt used are indicated in figure 3(e). The extent of porous surface could be varied by sealing part of the porous surface with pressure-sensitive tape 0.003 inch thick.

Pumping and Duct System

A drawing of the pumping and duct system is shown in figure 4. The suction air was drawn through the porous surface into the flaps which served as ducts carrying the air into the plenum chamber. After going through the pump, it was expelled through exhaust ducts located under the fuselage. The pumps were modified aircraft engine superchargers and were driven by variable-speed electric motors. The suction air-flow quantities were measured by finding the difference in pressure between the air in the plenum chambers and in the pump inlets. The system was calibrated with a standard A.S.M.E. intake orifice.

TESTING AND PROCEDURE

Tests at Varying Angle of Attack

Tests were made for an angle-of-attack range of -2° to 24°. For the model with horizontal tail off, tests were made with leading-edge-flap deflections of 0°, 31°, 41°, and 51°, combined with trailing-edge-flap deflections of 0°, 50°, and 60°.

Most of the tests were made either with area suction on both the leading- and trailing-edge-flap knees or without area suction on either of the flaps. For a few flap-deflection combinations, suction was applied to the trailing-edge flap but not to the leading-edge flap. For both the leading- and trailing-edge flaps with area suction, testing at variable angle of attack was done with a constant pump speed. The pump speeds used were those required to produce suction flow quantities approximately 100 percent and 30 percent greater than the critical flow quantity for the leading- and trailing-edge flaps, respectively. (For definition of C_{Q_c}, see subsequent discussion.) Porous area configurations for which data are presented herein are listed in table I. To expedite testing, no attempt was made to maintain the same porous area configuration for all variable-angle-of-attack tests. This procedure is believed justified since it was found that lift was fairly independent of small changes in porous opening and porosity for the large porous opening and excess flow quantities used. All suction-off data were obtained with the porous surfaces sealed.

A limited test was made on the model for $\delta_n = 41^\circ$ and $\delta_f = 60^\circ$ with the unswept horizontal tail installed at -2° incidence.

Force and moment data, as well as duct and plenum-chamber pressures, were obtained for all suction-on configurations investigated. For some of the configurations, external wing chordwise pressure distributions were obtained.

Tests at Constant Angle of Attack

Force and moment data were obtained for the model with varying flow quantities at given angles of attack in order to determine C_{Q_c} for various porous area configurations. The data were usually determined by decreasing the flow quantity from a high value to a low value. To check hysteresis effects on the lift characteristics, data were taken with increasing values of C_Q in several cases and no significant differences were observed from data obtained with decreasing values of C_Q.

In attempts to reduce the suction air flow required, the extent of porous area was varied for the trailing-edge flaps. For the leading-edge flap, only grade 2 felt was used. For the 50° deflected trailing-edge flap, only grade 1 felt was used. For the 60° trailing-edge flap, in addition to grade 1 felt, grade 2 felt and combinations of the two types of felt over the span of the flap were investigated as a means of reducing flow requirements.

Additional tests to determine the effect of airspeed on the suction flow requirements of the trailing-edge flap were made for $\delta_n = 40^\circ$ and $\delta_f = 50^\circ$ and one porous area configuration. These variable C_Q tests were made at about 0° angle of attack and free-stream velocities of 130, 159, and 183 feet per second.

Test Conditions

The Reynolds number of the tests, aside from the tests with the higher free-stream velocities mentioned above, was 9.4×10^6 which corresponded to a dynamic pressure of 20 pounds per square foot and a Mach number of 0.11.

CORRECTIONS TO DATA

All data were corrected for air-stream inclination and for wind-tunnel wall effects, the latter correction being that for a wing of the same span having elliptic loading and with an unswept plan form. The corrections added were as follows:

$$\alpha_T = 0.696\ C_L$$

$$C_{D_T} = 0.0122\ C_L^2$$

For the data with the horizontal tail installed, a correction for additional downwash at the hinge line of the tail (at the model plane of symmetry) was made as follows:

$$C_{m_T} = 0.0139\ C_L$$

Tares due to support strut interference were not applied.

All flow coefficients were corrected to standard sea-level air conditions. The effect of the thrust of the exhaust jets on the aerodynamic data was found to be negligible.

RESULTS AND DISCUSSION

The Effect of Leading- and Trailing-Edge Flap Deflection

The force and moment characteristics of the model (tail off) for several combinations of leading- and trailing-edge-flap deflections are presented in figures 5 and 6 for the model without and with area suction applied to both leading- and trailing-edge flaps. Chordwise pressure distributions for three spanwise stations are presented in figures 7 and 8 for the model with and without the leading-edge flap deflected. For $\delta_n = 41^\circ$ and $\delta_f = 60^\circ$, chordwise pressure distributions for several spanwise stations are presented in figure 9 for four angles of attack. (All pressure data for the leading-edge flap, wing, and trailing-edge flap were plotted in directions normal to the respective chord lines.) The

approximate values of C_Q and P_p corresponding to the constant pump speeds held throughout the angle-of-attack range for the various model configurations are listed in table II.

Flap lift increments.- For the model with the leading-edge flaps undeflected, the variation of trailing-edge-flap lift increment with angle of attack is shown in figure 10. The pressure data of figure 7(a) and tuft observations (not presented herein) show that at $\alpha = 0^\circ$ leading-edge flow separation has occurred. With increasing angle of attack above 0°, the chordwise extent of the leading-edge flow separation increased and resulted in a rapid decrease in trailing-edge-flap lift increment. As is shown in figure 10, for angles of attack up to that of $C_{L_{max}}$, these decreases in ΔC_L were caused essentially by loss in boundary-layer control. Therefore, leading-edge flow separation must be controlled before any substantial boundary-layer control effectiveness is to be realized on the trailing-edge flap for this type of wing in the medium to high angle-of-attack range.

To study the effect of controlling leading-edge flow separation, the leading-edge flaps were deflected with and without area suction. For the model with the leading-edge flap deflected, the variation of trailing-edge-flap lift increment with angle of attack is shown in figure 11. Substantial flap lift increments with suction off and on were maintained up to angles of attack of 16° or more. The pressure data of figures 7 and 8 demonstrate the effectiveness of the leading-edge flap with area suction in delaying the chordwise progression of flow separation from the leading edge. Even though the flow separation does appear on the leading edge, attached flow is maintained over the knee of the leading-edge flap up to high angles of attack. As shown by the pressure data of figure 8, the trailing-edge-flap lift increment does not drop radically until an angle of attack is reached (close to that of $C_{L_{max}}$) where flow separation spreads over the leading-edge-flap knee.

High-lift characteristics.- For the model with area suction applied to the trailing-edge flaps, it was found that the leading-edge flaps were needed to obtain a value of $C_{L_{max}}$ substantially greater than the value of C_L found for $\alpha = 0^\circ$. Values of $C_{L_{max}}$ for the model with the tail off obtained with several flap-deflection combinations are listed in the following table:

Trailing-edge flap		Leading-edge flap		$C_{L_{max}}$
δ_f, deg	Suction	δ_n, deg	Suction	
0	off	0	off	0.78
50	off	0	off	1.24
50	on	0	off	1.30
60	off	0	off	1.24
60	on	0	off	1.30
0	off	41	off	1.21
0	off	41	on	1.29
50	off	41	off	1.45
50	on	41	on	1.76
60	off	41	off	1.43
60	on	41	off	1.60
60	on	41	on	1.78

A comparison of the values shown in the table indicates that little or no increase in $C_{L_{max}}$ was obtained by increasing the trailing-edge-flap deflection from 50° to 60° for any of the leading-edge-flap conditions considered. However, a 35-percent increase in $C_{L_{max}}$ was obtained by deflecting the leading-edge flap with area suction for the model with area suction applied to the deflected trailing-edge flaps.

The variation of $C_{L_{max}}$ with δ_n is shown in figure 12 for the two trailing-edge-flap deflections. The figure demonstrates the decreasing advantage of higher leading-edge-flap deflections as δ_n approached 50°.

Figure 13 shows the effect of applying area suction to the leading-edge flap on the lift characteristics of the model. For angles of attack up to 8°, little, if any, added lift due to suction was obtained for either the 31° or 41° leading-edge-flap deflection. For angles of attack above 8°, the advantage of area suction was apparent only for the 41° leading-edge-flap deflection.

Comparison with theory.- The trailing-edge-flap effectiveness is summarized in figure 14 for the model at $\alpha = 0°$. The experimental data from which the values presented in figure 14 were taken were obtained with approximately 50-percent excess suction air flow. Also presented in the figure is the variation of flap effectiveness with flap deflection as predicted by the theory of reference 5. The value of α_δ used for the calculations was the theoretical value of 0.65 taken from figure 3 of that reference. With the nose flap deflected 41°, applying area suction to the trailing-edge flap increased the flap lift increment from 48 to 91 percent of theory for $\delta_f = 50°$ and from 44 to 81 percent of theory for $\delta_f = 60°$.

Sources of loss in flap lift.- Two regions on the trailing-edge flap existed at which the flow could not be attached using area suction and

which evidently contributed to the discrepancy between the suction-on experimental data and the corresponding theoretical values. Early in the investigation, it was found from tuft observations and pressure measurements that for spanwise stations between $\eta = 0.45$ and 0.60, a considerable amount of separated flow occurred on the flap even at high suction flow quantities. Boundary-layer measurements showed that just forward of the porous area, large values of the boundary-layer shape parameter (ratio of displacement thickness to momentum thickness of the boundary layer) existed at these wing stations compared to the values found at other spanwise locations. Insufficient suction inflow velocity over the porous area in this region was the probable cause for the flow separation on the flap. The other region of separated flow existed adjacent to the fuselage and, as explained in reference 6, was evidently caused by the low-energy air in the fuselage boundary layer not being able to negotiate the high adverse pressure gradient induced by the presence of the knee of the flap.

Use of turning vanes.- To improve flow over regions on the flap near the fuselage, turning vanes were installed for a brief part of the test at the knee of the flap as suggested by the information in reference 6. The span of the vanes (approximately 5 inches) was slightly larger than the thickness of the fuselage boundary layer at that point. The effect of vanes on the lift characteristics of the model for $\delta_n = 41^\circ$ and $\delta_f = 60^\circ$ is shown in figure 15. The triple vanes increased the flap lift increment from 81 percent to 92 percent of the theory of reference 5 (see fig. 14).

Suction Requirements

Trailing-edge flaps.- Typical variations of ΔC_L versus C_Q are shown in figure 16 for δ_f of 50° and 60°; the curves represent porous area configurations for which the flow requirements were found to be close to the minimum obtained for the corresponding flap deflection. For both flap deflections, data are shown which were obtained with the more porous felt (grade 1). Also shown in figure 16 are data representing the best porous area configuration used during an attempt to reduce the flow requirements by changing the spanwise porosity distribution. It may be seen from the figure that there is a critical value of flow coefficient above which significant increases in lift cannot be obtained by any reasonable increase of suction flow quantity. The coefficients corresponding to this value are designated herein as the critical flow coefficients, C_{Q_c}, and, as in reference 3, are determined as the value at which the nearly linear part of the curve begins. Values of C_{Q_c} were estimated by use of the method described in reference 3[1] and are indicated on the curves of figure 16.

[1]The method outlined in reference 3 may be stated mathematically as

$$C_Q = (C_Q)_1 \frac{(S_R/S)\cos \Lambda_f}{(S_R/S)_1 \cos (\Lambda_f)_1}$$

where reference values are indicated by the subscript 1.

These estimated values are also compared in the following table with the approximate experimental values of the present investigation indicated by the data of figure 16.

δ_f, deg	Experimental $\delta_n = 41^\circ$	Estimated
50	0.0008	0.00068
60	.0013	.00110

The experimental values are those obtained with the grade 1 felt which was of approximately the same porosity as that with which the reference data used in the method were obtained.

The small effects of free-stream velocity on the variation of ΔC_L with C_Q and P_p are shown in figure 17.

Leading-edge flaps.- As has been mentioned previously, suction on the leading-edge flaps became necessary for the 41° deflection at angles of attack above 9° (see fig. 13).

The felt design for the three leading-edge flap deflections investigated was of variable porosity chordwise and proved to yield adequate boundary-layer control for values of C_{Q_c} as small as 0.0003. Suction flow data for the leading-edge flap are not presented herein but it should be mentioned that values of C_{Q_c} for both $\delta_n = 41^\circ$ and 51° at higher angles of attack varied from 0.0002 to 0.0003.

Stability Characteristics of the Model

Comparison of the suction-on and suction-off pitching-moment data of figures 5 and 6 for the tail-off model indicates that the use of boundary-layer control by porous area suction causes extreme destabilizing pitching-moment variations, as well as large negative pitching moments.

Results obtained from brief tests with a thin unswept horizontal tail are presented in figure 18. To augment trailing-edge-flap effectiveness, the triple-vane configuration mentioned above was installed at the flap. In order to trim the model, a split flap was installed on the upper surface of the tail. It is evident that the horizontal tail contributes favorably to the pitching-moment variation of the model.

[redacted]

CONCLUDING REMARKS

The results obtained from tests of an airplane model with an aspect-ratio-3 unswept wing of thin wing section indicated the following:

Application of porous area suction to the trailing-edge flap approximately doubled the flap lift increment obtained at 0° angle of attack. With area suction on the trailing-edge flap, and with the leading-edge flap deflected 41°, trailing-edge-flap lift increments were obtained which were 91 and 81 percent of theoretical values (NACA Rep. 1071) for flap deflections of 50° and 60°, respectively. The flow requirements of the trailing-edge flap were close to predictions based on data obtained from tests on a 35° swept-wing model reported in NACA RM A53E06.

For angles of attack above 0°, leading-edge-flap deflection was required to limit widespread leading-edge flow separation. The leading-edge flow separation which appeared on the undeflected leading edge caused large reductions in trailing-edge-flap lift increment. With the trailing-edge flap deflected 60° (suction on), area suction on the leading-edge flap was not required for a deflection of 31° but was required for the 41° flap deflection at angles of attack above 8°. For the model with the tail off, the use of boundary-layer control on the trailing-edge flap increased destabilizing pitching-moment changes. However, installation of a horizontal tail markedly reduced these adverse pitching moments.

Ames Aeronautical Laboratory
National Advisory Committee for Aeronautics
Moffett Field, Calif., Apr. 23, 1956

REFERENCES

1. Delany, Noel K., and Hayter, Nora-Lee F.: Low-Speed Investigation of a 0.16-Scale Model of the X-3 Airplane - Longitudinal Characteristics. NACA RM A50G06, 1950.

2. McKee, John W., and Riebe, John M.: An Investigation of a 0.16-Scale Model of the Douglas X-3 Airplane to Determine Means of Improving the Low-Speed Longitudinal Stability and Control Characteristics. NACA RM L52H01, 1952.

3. Cook, Woodrow L., Holzhauser, Curt A., and Kelly, Mark W.: The Use of Area Suction for the Purpose of Improving Trailing-Edge Flap Effectiveness on a 35° Sweptback Wing. NACA RM A53E06, 1953.

4. Holzhauser, Curt A., and Martin, Robert K.: The Use of a Leading-Edge Area-Suction Flap to Delay Separation of Air Flow From the Leading Edge of a 35° Sweptback Wing. NACA RM A53J26, 1953.

5. DeYoung, John: Theoretical Symmetrical Span Loading Due to Flap Deflection for Wings of Arbitrary Plan Form at Subsonic Speeds. NACA Rep. 1071, 1952.

6. Kelly, Mark W., and Tolhurst, William H., Jr.: The Use of Area Suction to Increase the Effectiveness of a Trailing-Edge Flap on a Triangular Wing of Aspect Ratio 2. NACA RM A54A25, 1954.

TABLE I.- POROUS AREA CONFIGURATIONS
[See figure 3 for notation description]

(a) Leading-edge flap; η_I = 0.15 to η_O = 1.0; a = 0°

δ_n, deg	Porous area extent
31	Total opening, 0.88 inch, constant along span
41	S = 0.5 inch
51	Total opening, 1.06 inch, constant along span

(b) Trailing-edge flap

Porous area configuration	δ, deg	Porous area extent		Felt, spanwise extent		Felt grade
		a, deg	s	η_I	η_O	
1	50	0	2.5 in.	0.15	0.75	1
2	50	15	1.0 in.	.15	.75	1
3	60	12	.5 in.	.15	.75	1
4	60	12	1.5 in.	.15	.75	1
5	60	12	3.0 in.	.15	.32	2
		18	1.5 in.	.32	.60	1
		12	3.0 in.	.60	.75	2
6	60	12	5 percent	.15	.75	2

TABLE II.- AVERAGE VALUES OF PLENUM CHAMBER PRESSURE AND FLOW COEFFICIENTS HELD THROUGH THE ANGLE-OF-ATTACK RANGE

Figure number	δ_n, deg	δ_f, deg	Trailing-edge porous-area configuration	Leading-edge flap		Trailing-edge flap	
				C_Q	P_p	C_Q	P_p
6(a)	31	0[1]	sealed	0.0008	-11.5	- - -	- - -
	41	0[1]	sealed	.0008	-11.5	- - -	- - -
6(b)	0[1]	50	2	- - -	- - -	0.0015	-10.6
	31	50	2	.0008	-11.5	.0014	-10.5
	41	50	2	.0010	-14.5	.0015	-10.6
	51	50	2	.0006	-12.7	.0015	-10.5
6(c)	0[1]	60	6	- - -	- - -	.0017	-13.5
	31	60	4	.0008	-11.5	.0018	-14
	41	60	4	.0011	-14.5	.0016	-13.2
7	0[1]	60	6	- - -	- - -	.0017	-13.6
8	31	50	2	.0008	-11.5	.0014	-10.5
	41	50	2	.0010	-15.0	.0015	-10.6
	51	50	2	.0006	-12.7	.0015	-10.5
9	41	60	5	.0006	-11.5	.0016	-13.6
13	0[1]	60	6	- - -	- - -	.0017	-13.5
	31[1]	60	3	- - -	- - -	.0017	-13.6
	31	60	3	.0008	-11.5	.0017	-13.6
	41[1]	60	4	- - -	- - -	.0016	-13.2
	41	60	4	.0011	-14.5	.0016	-13.2
15	41	60	5	.0006	-12.0	.0016	-13.5
18	41	60	5	.0005	-11.5	.0017	-13.7

[1]Porous area on flap sealed.

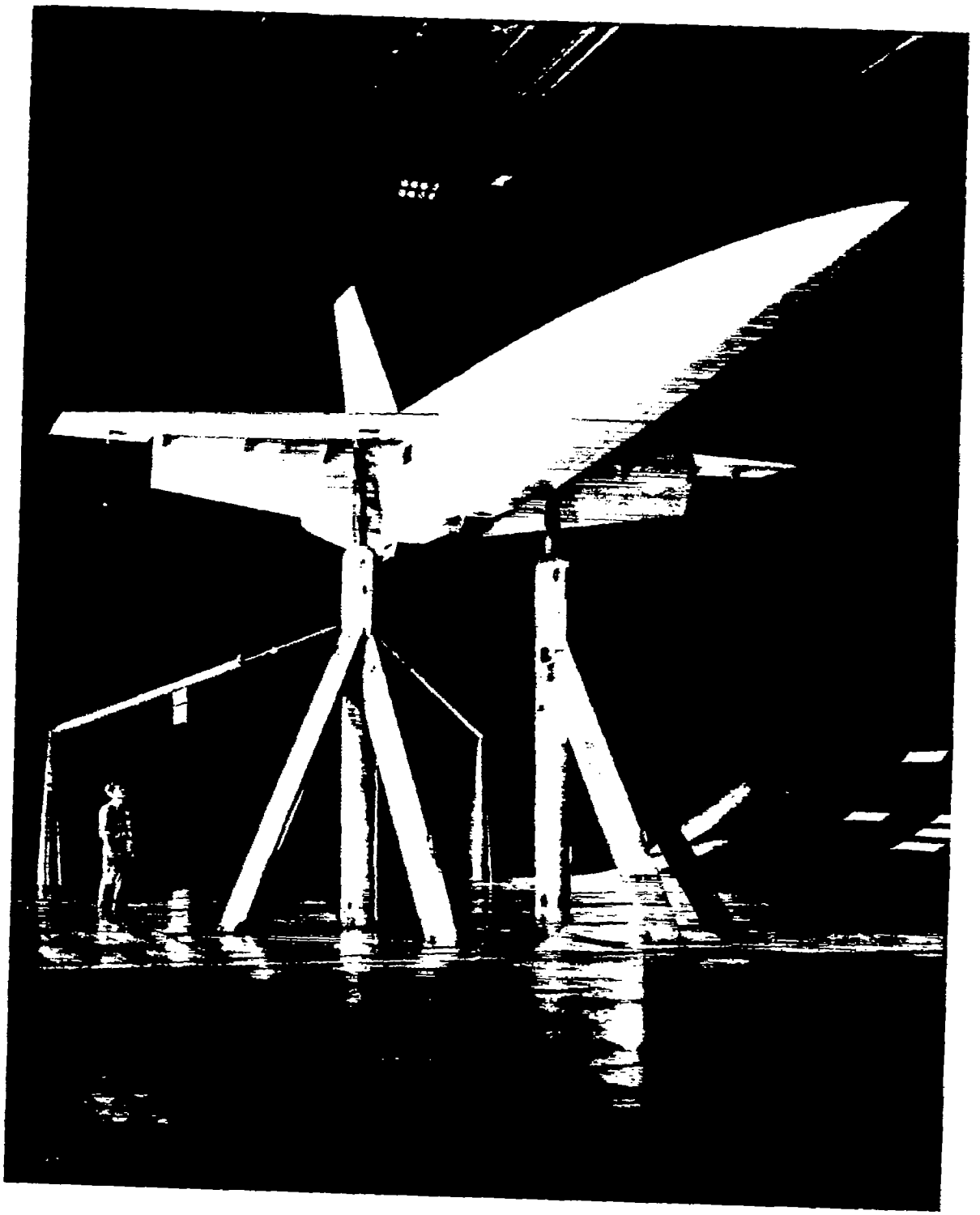

A-19567

Figure 1.- View of the model in the Ames 40- by 80-foot wind tunnel.

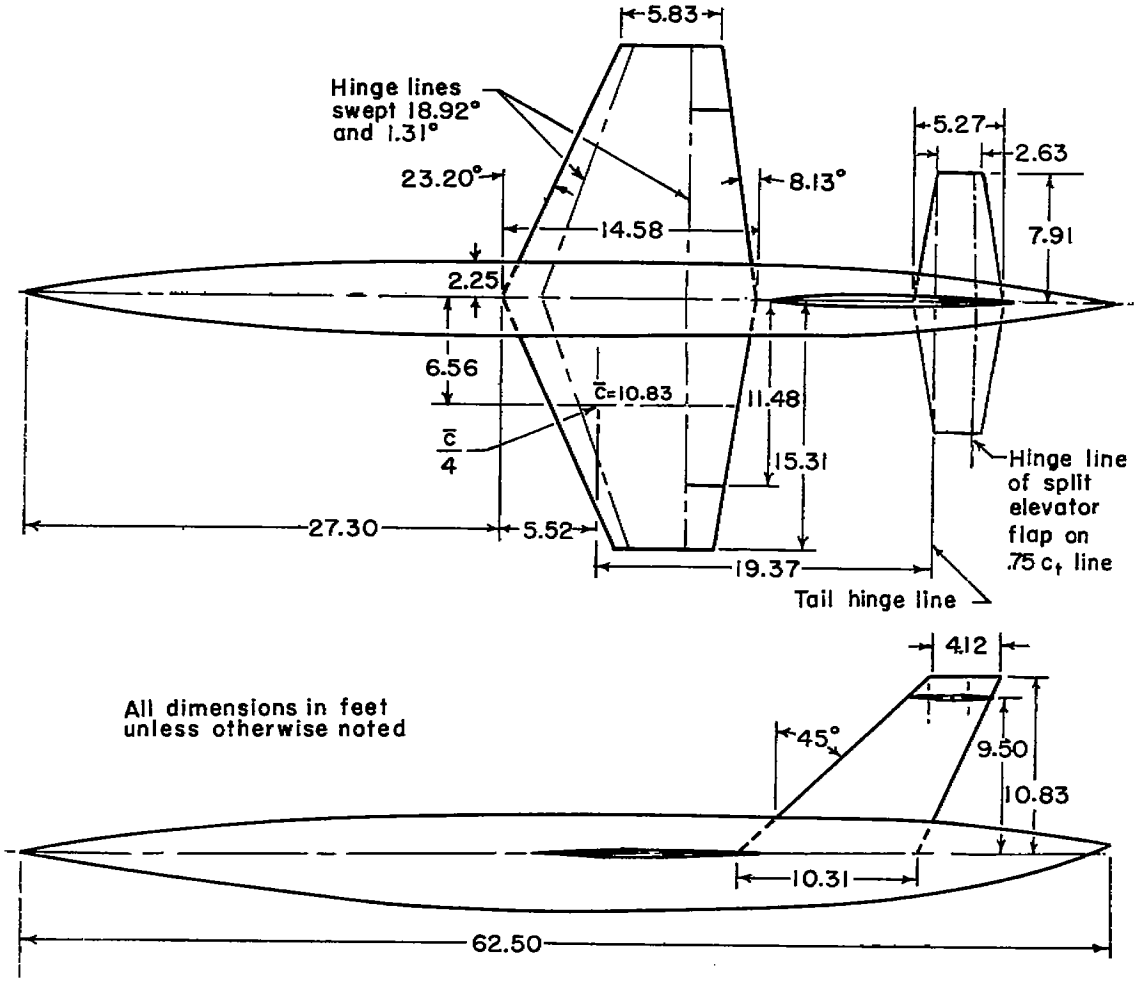

Wing Geometry	
Aspect ratio	3.0
Taper ratio	0.4
Sweep of quarter-chord line	15.9°
Dihedral	0°
Twist	0°
Area, square feet	312.5
Wing section	4.2 % thick modified double wedge

(a) The complete model.

Figure 2.- Geometric characteristics of the model.

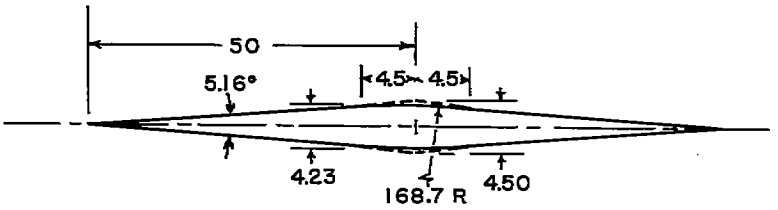

Typical wing section
Dimensions in percent wing chord

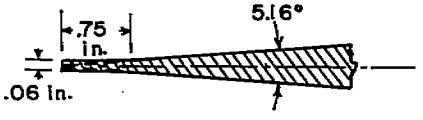

Typical of leading and trailing edge

(b) The wing section.

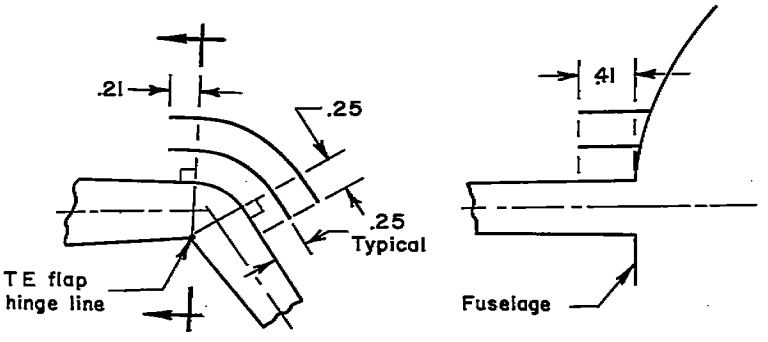

Double vane

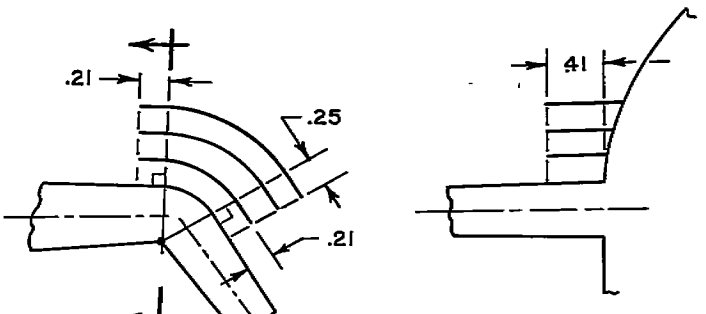

All dimensions shown in feet
All vanes .06 inch thick
Left side shown, right side opposite

Triple vane

(c) Turning vanes.

Figure 2.- Continued.

CONFIDENTIAL

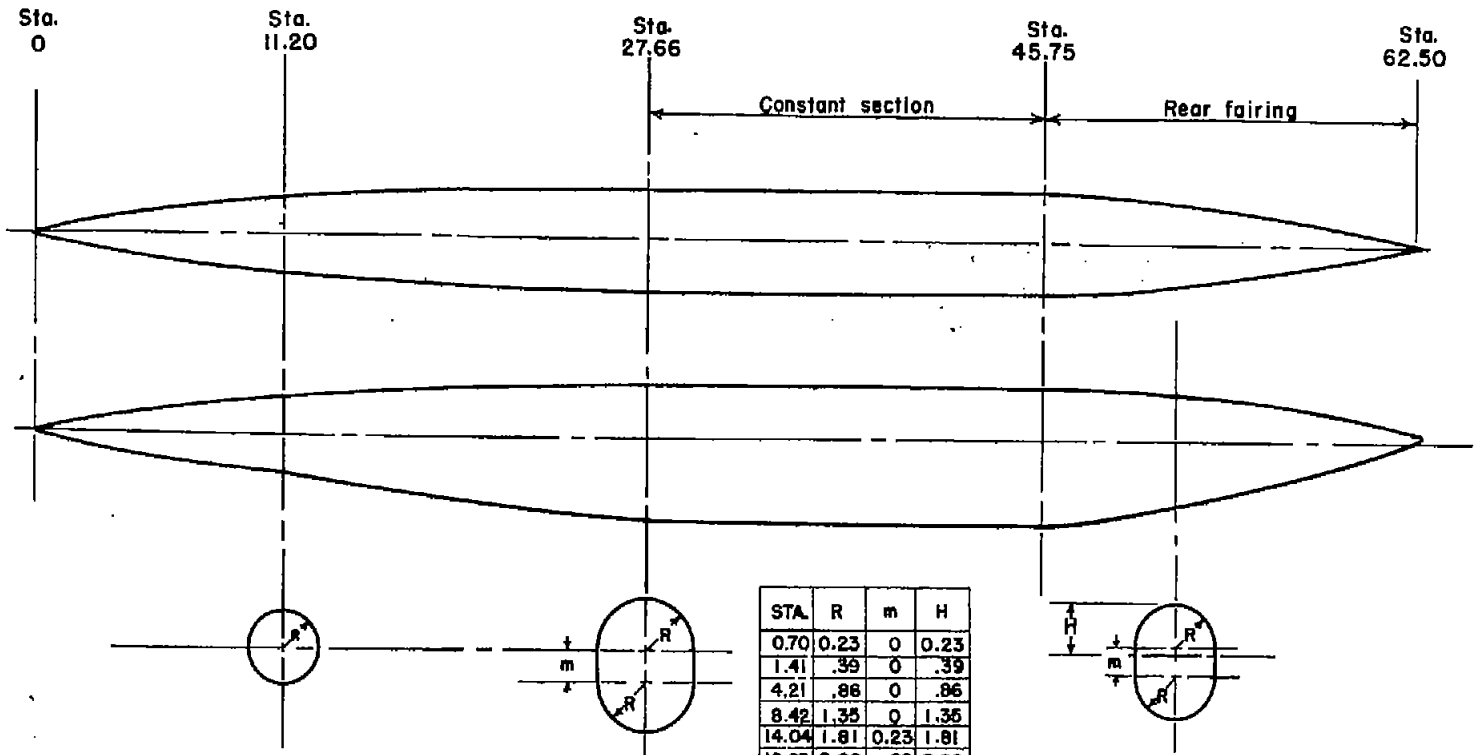

STA.	R	m	H
0.70	0.23	0	0.23
1.41	.39	0	.39
4.21	.86	0	.86
8.42	1.35	0	1.35
14.04	1.81	0.23	1.81
19.65	2.09	.69	2.09
27.66	2.25	1.33	2.25
47.75	2.18	1.28	2.22
49.75	2.02	1.17	2.15
51.75	1.80	1.03	2.00
53.75	1.57	.88	1.85
55.75	1.30	.76	1.65
57.75	1.00	.64	1.40
59.75	.67	.48	1.09
61.75	.25	.20	.60

(d) The fuselage.

Figure 2.- Concluded.

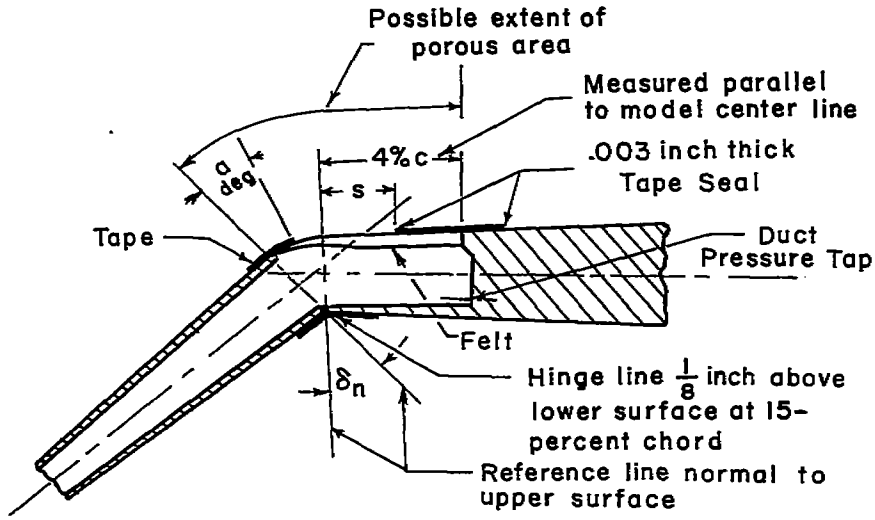

(a) Leading-edge flap.

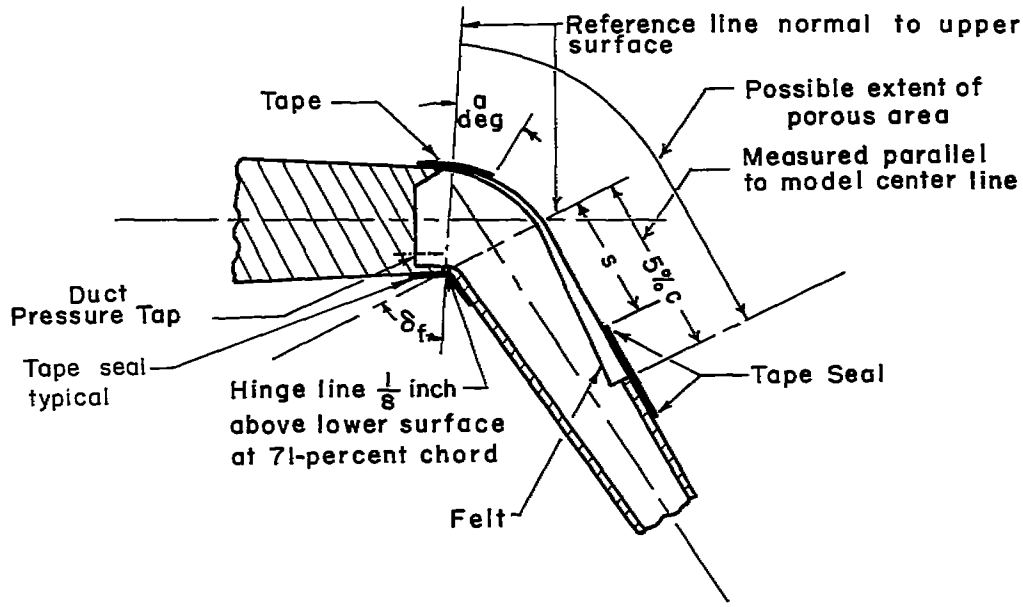

(b) Trailing-edge flap.

Figure 3.- Details of the porous surface of the model.

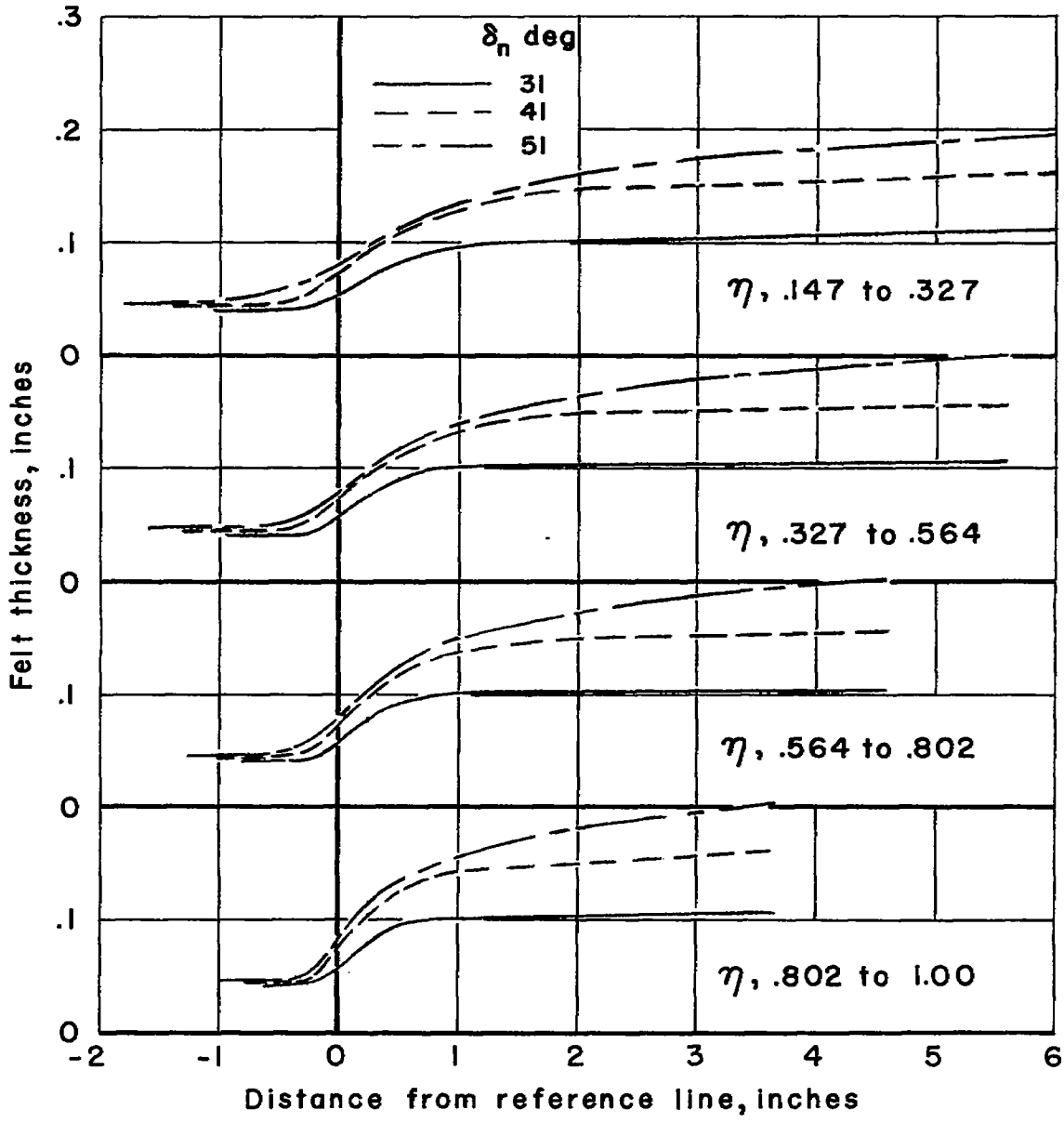

(c) Felt thickness distribution for leading-edge flap. Grade 2 felt.

Figure 3.- Continued.

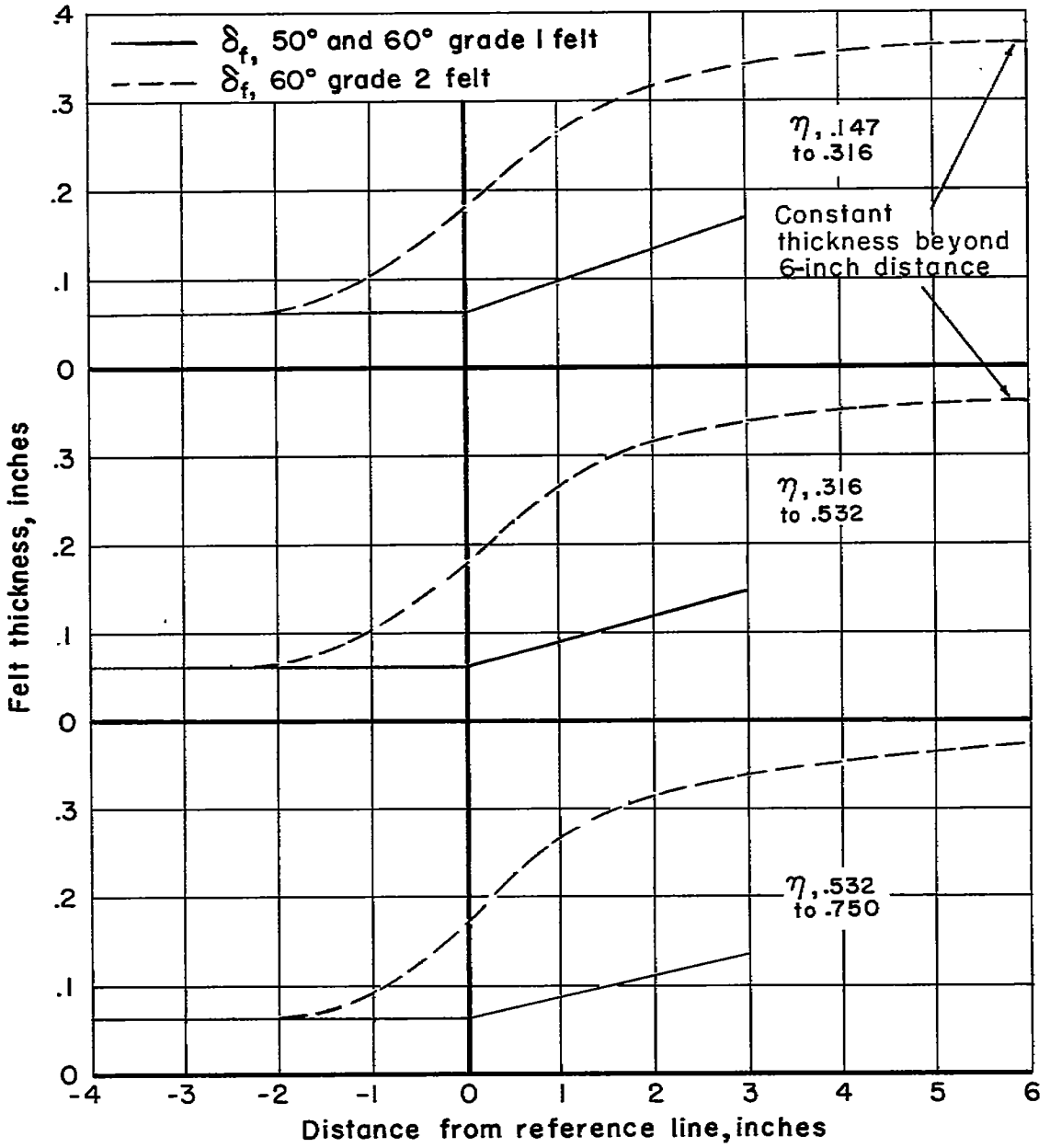

(d) Felt thickness distribution for trailing-edge flap.

Figure 3.- Continued.

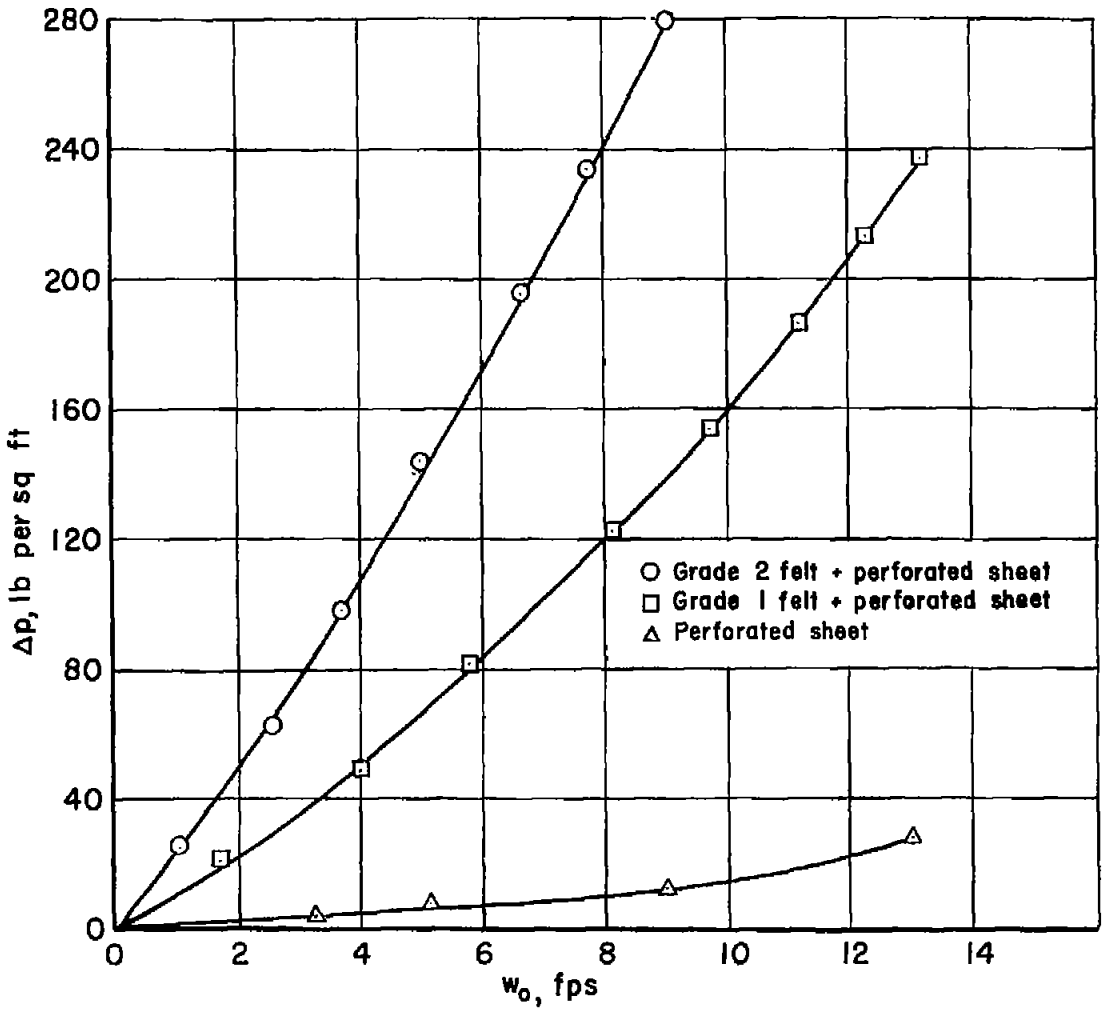

(e) Variations of suction inflow velocity with pressure differential across felt, one-quarter-inch thick.

Figure 3.- Concluded.

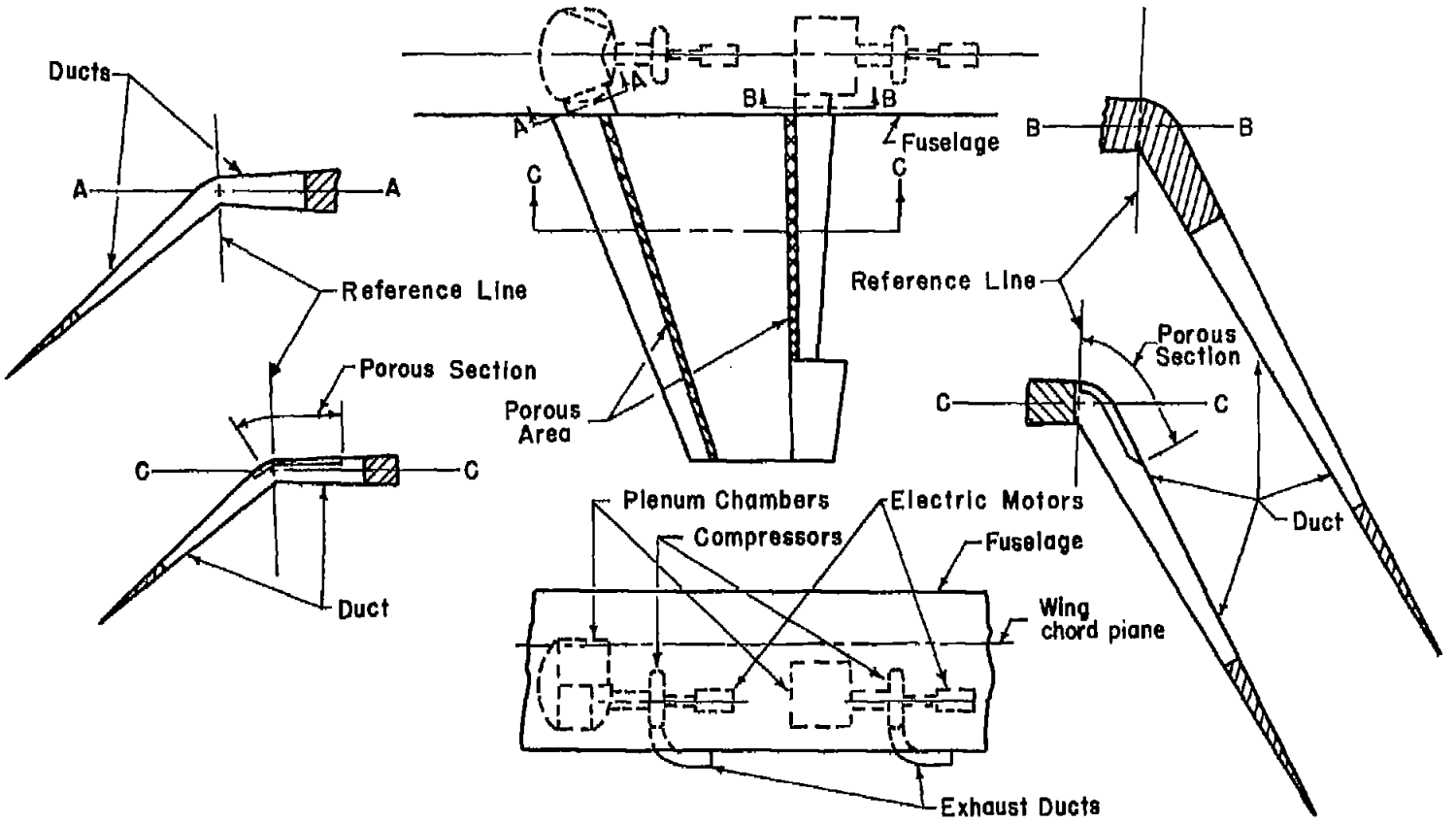

Figure 4.- Details of the model duct and pumping system.

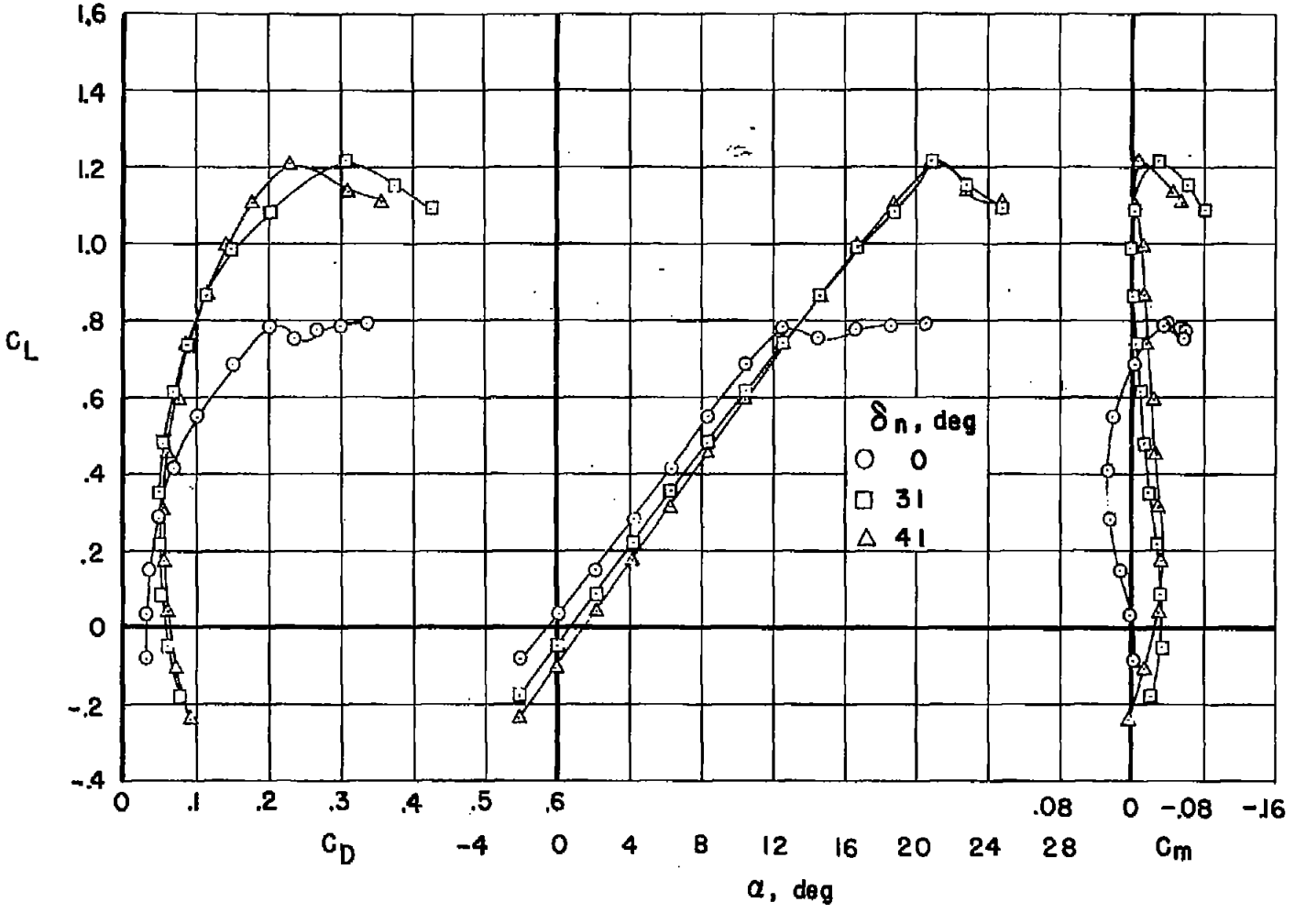

(a) $\delta_f = 0^\circ$

Figure 5.- The effect of leading-edge-flap deflection on the longitudinal characteristics of the model without suction on either the leading- or trailing-edge flap.

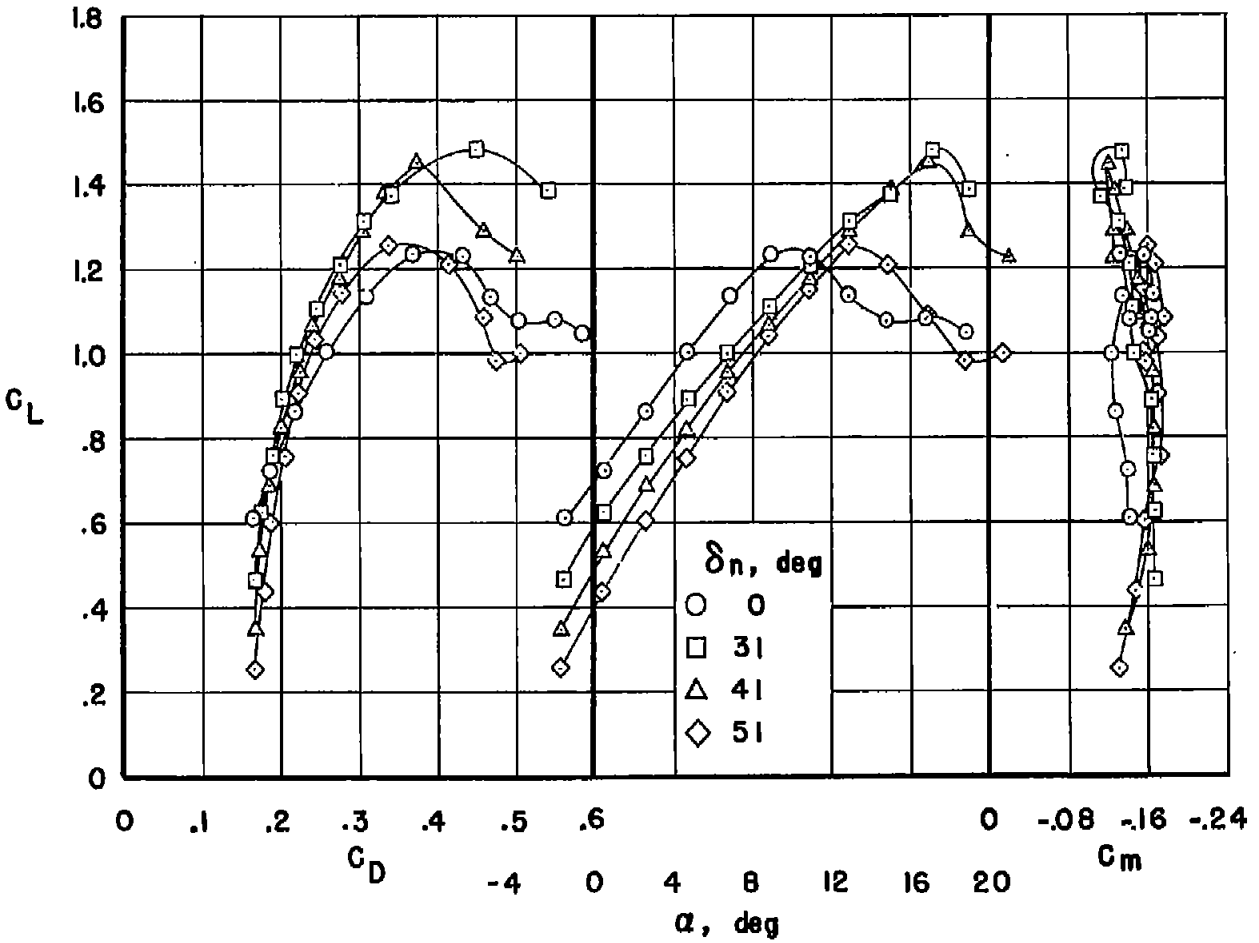

(b) $\delta_f = 50°$

Figure 5.- Continued.

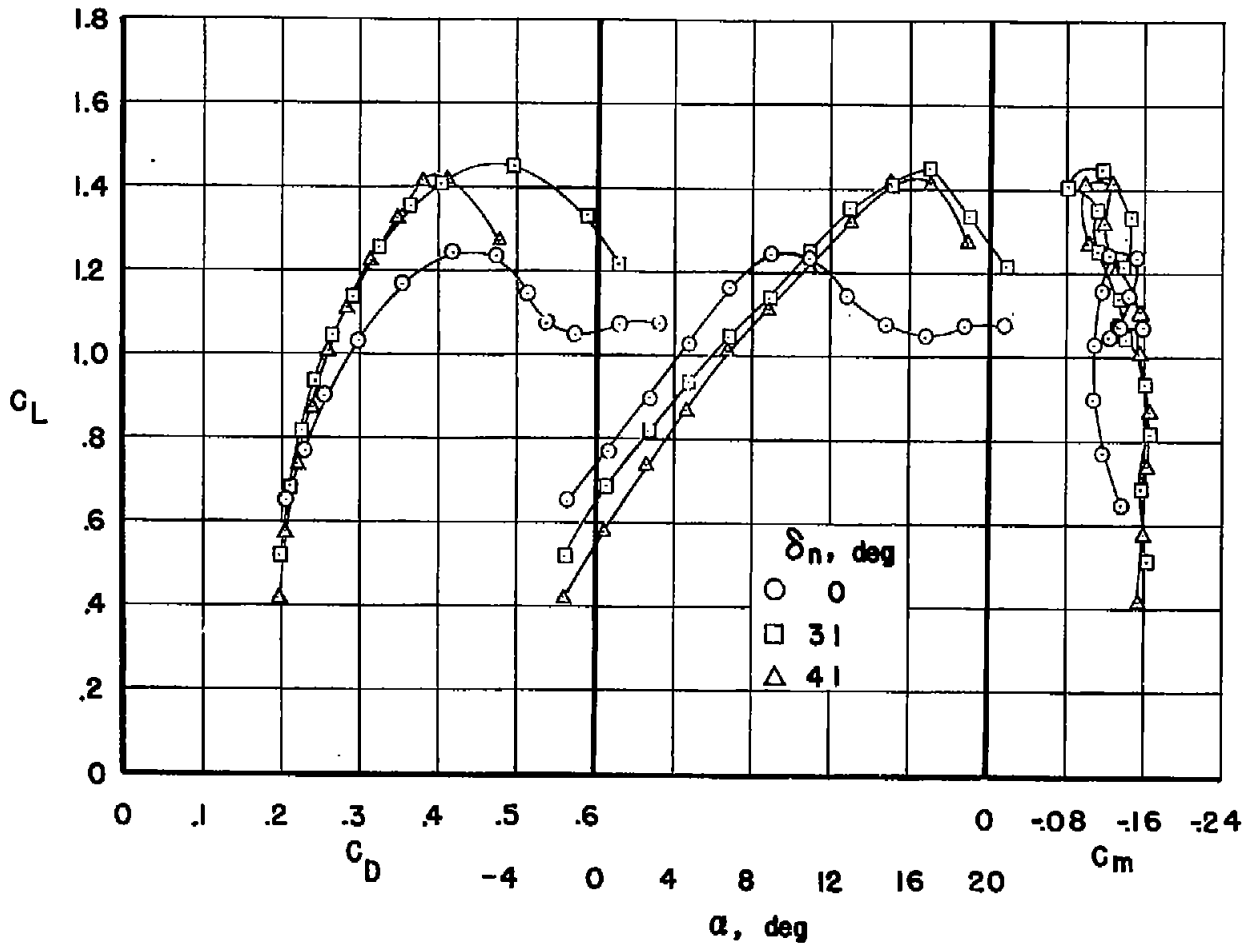

(c) $\delta_f = 60°$

Figure 5.- Concluded.

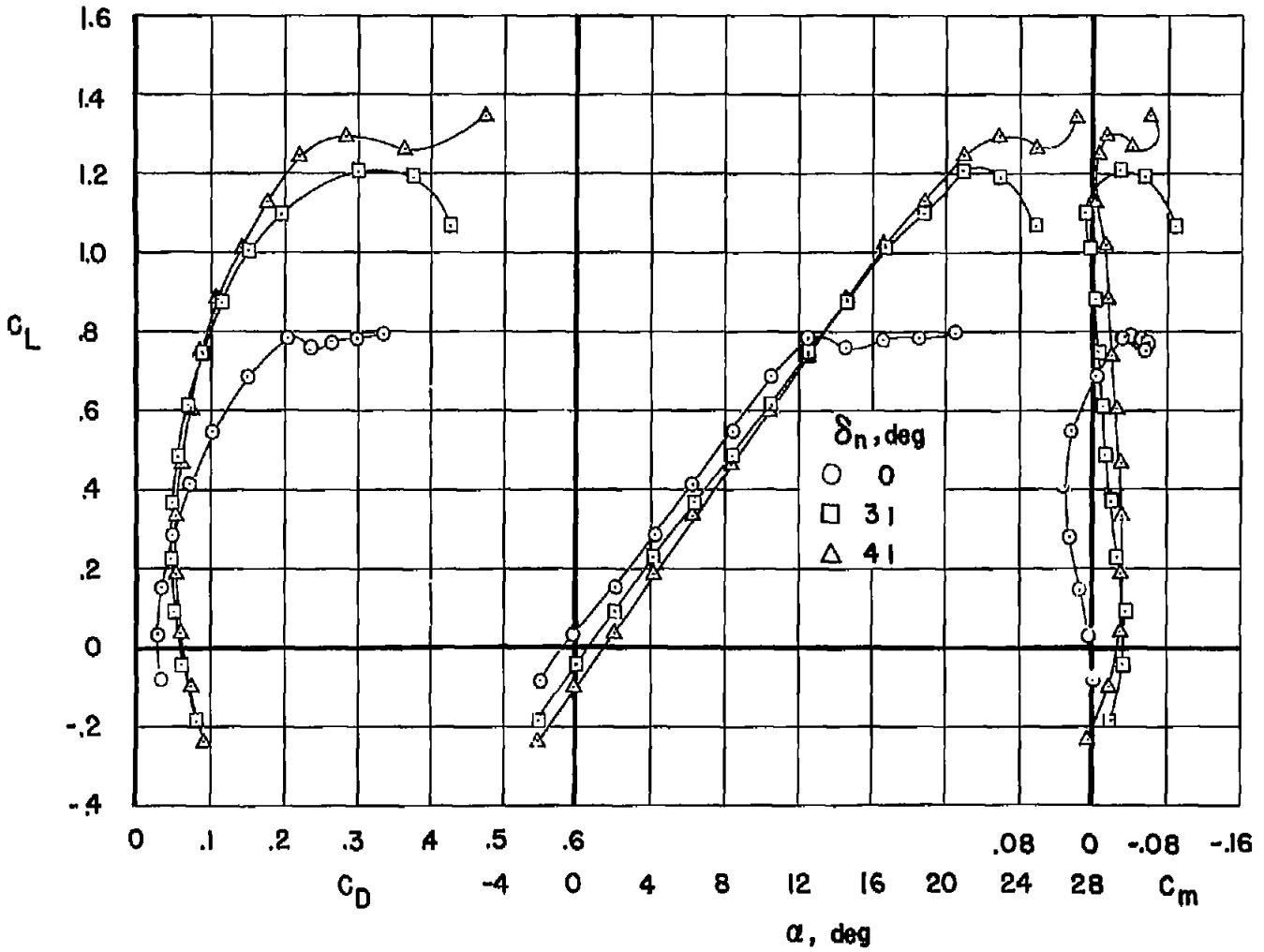

(a) $\delta_f = 0^\circ$

Figure 6.- The effect of leading-edge-flap deflection on the longitudinal characteristics of the model with suction on both the leading- and trailing-edge flaps. For porous area and suction air-flow conditions, see table II.

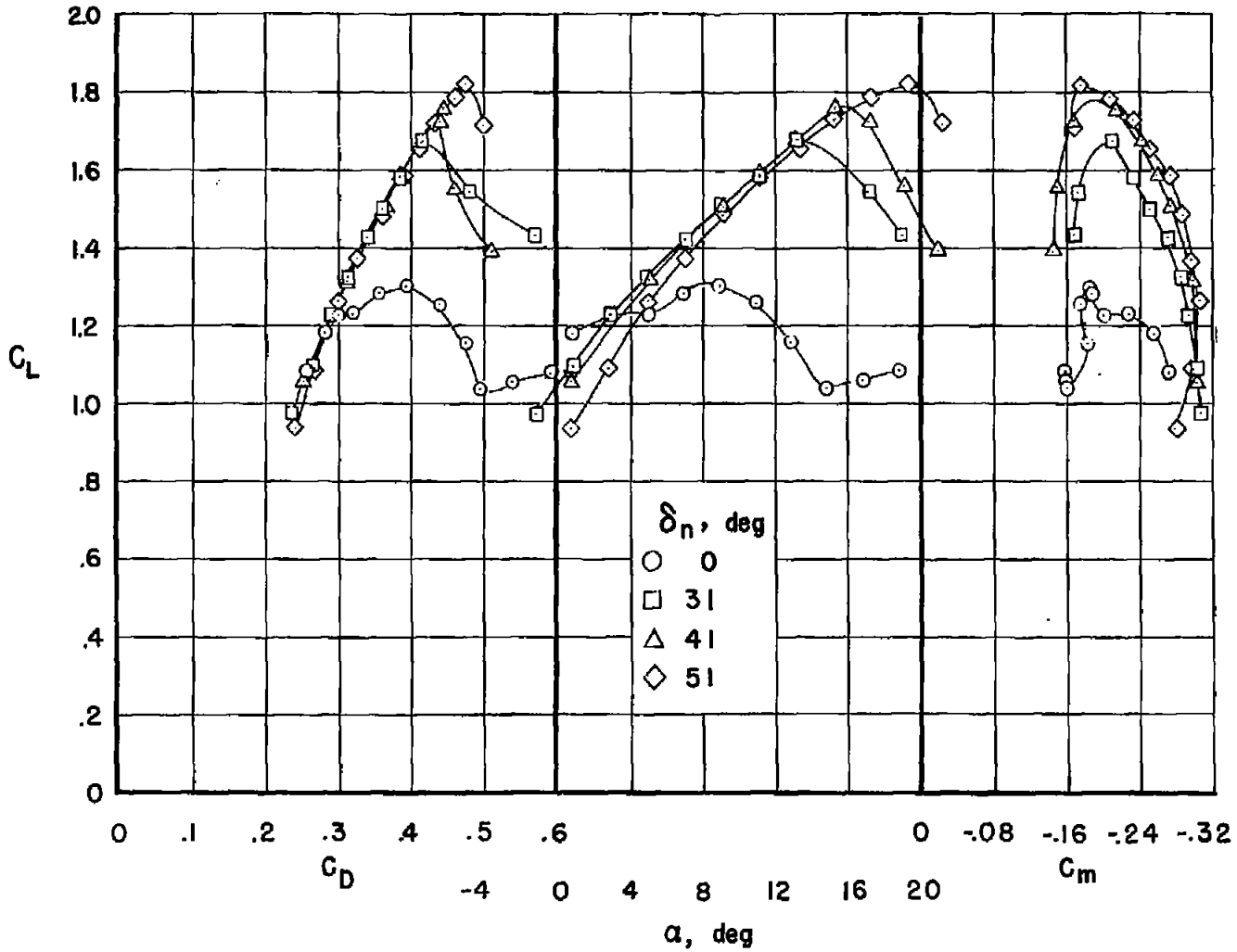

(b) $\delta_f = 50^\circ$

Figure 6.- Continued.

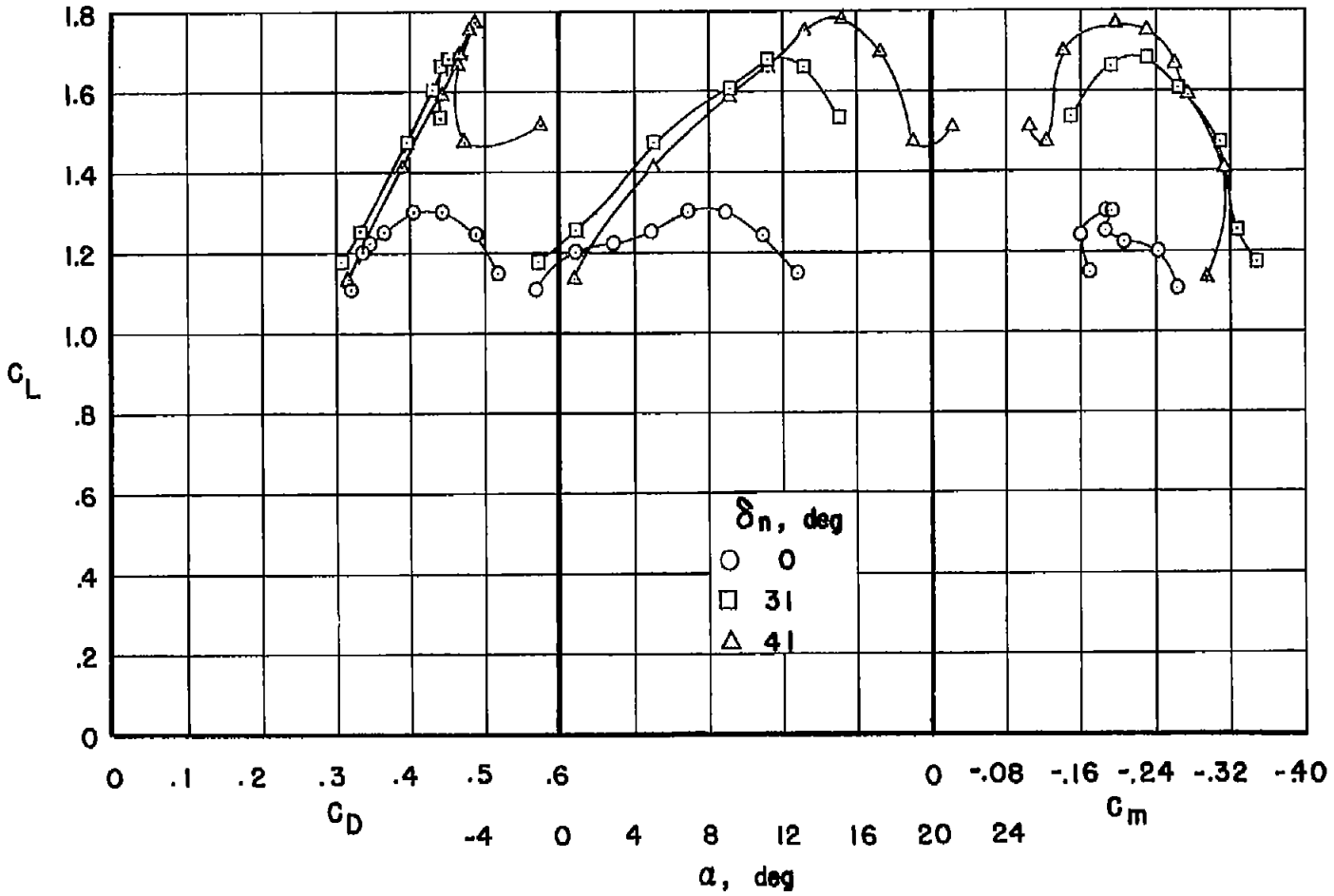

(c) $\delta_f = 60^\circ$

Figure 6.- Concluded.

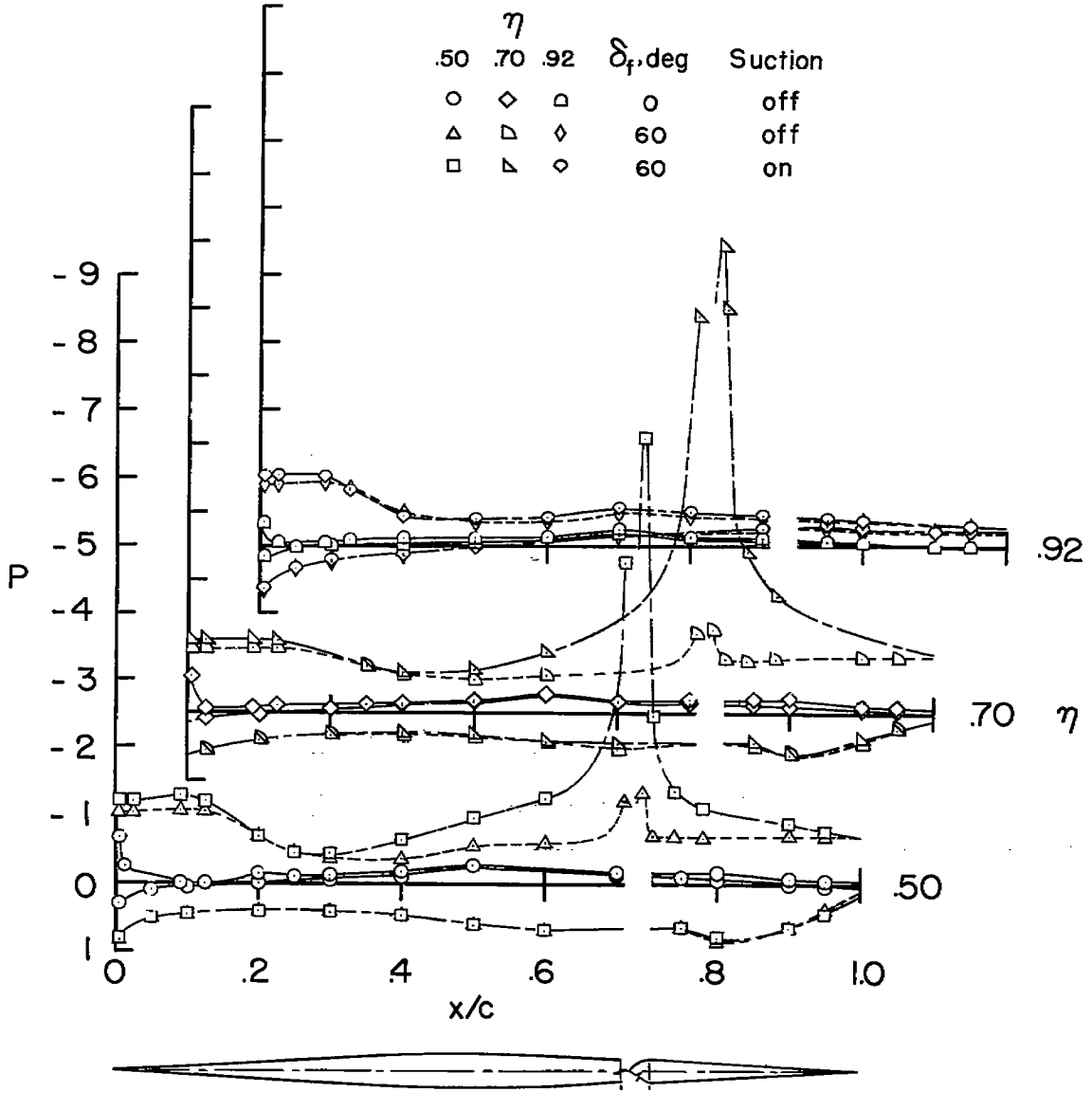

(a) $\alpha = 0.9^{\circ}$

Figure 7.- Chordwise pressure distributions at three spanwise stations with the leading-edge flap undeflected. For porous area and suction air-flow conditions, see table II. The x/c axis is broken at the value of x/c corresponding to the flap hinge.

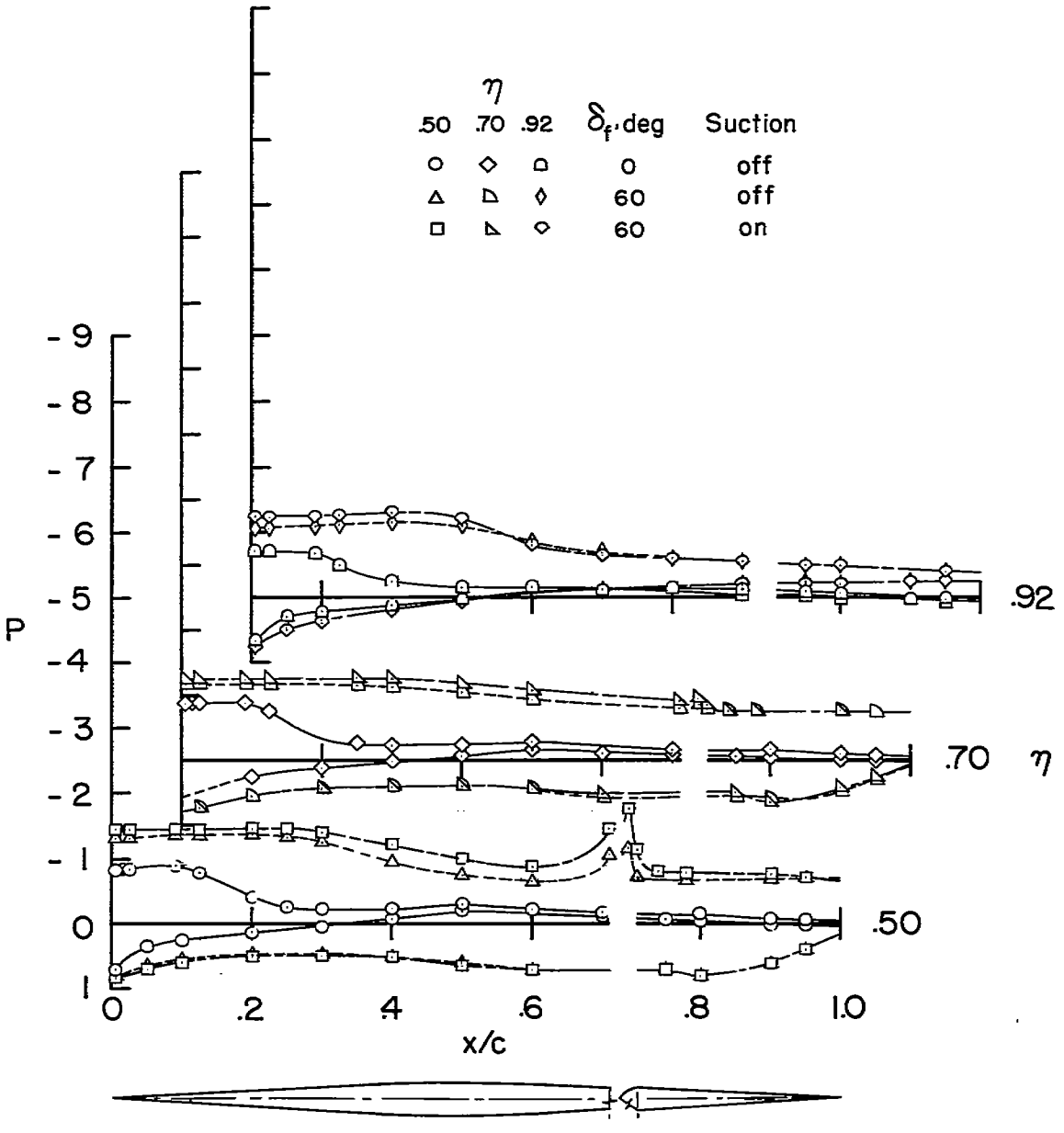

(b) $\alpha = 5.0^{\circ}$

Figure 7.- Continued.

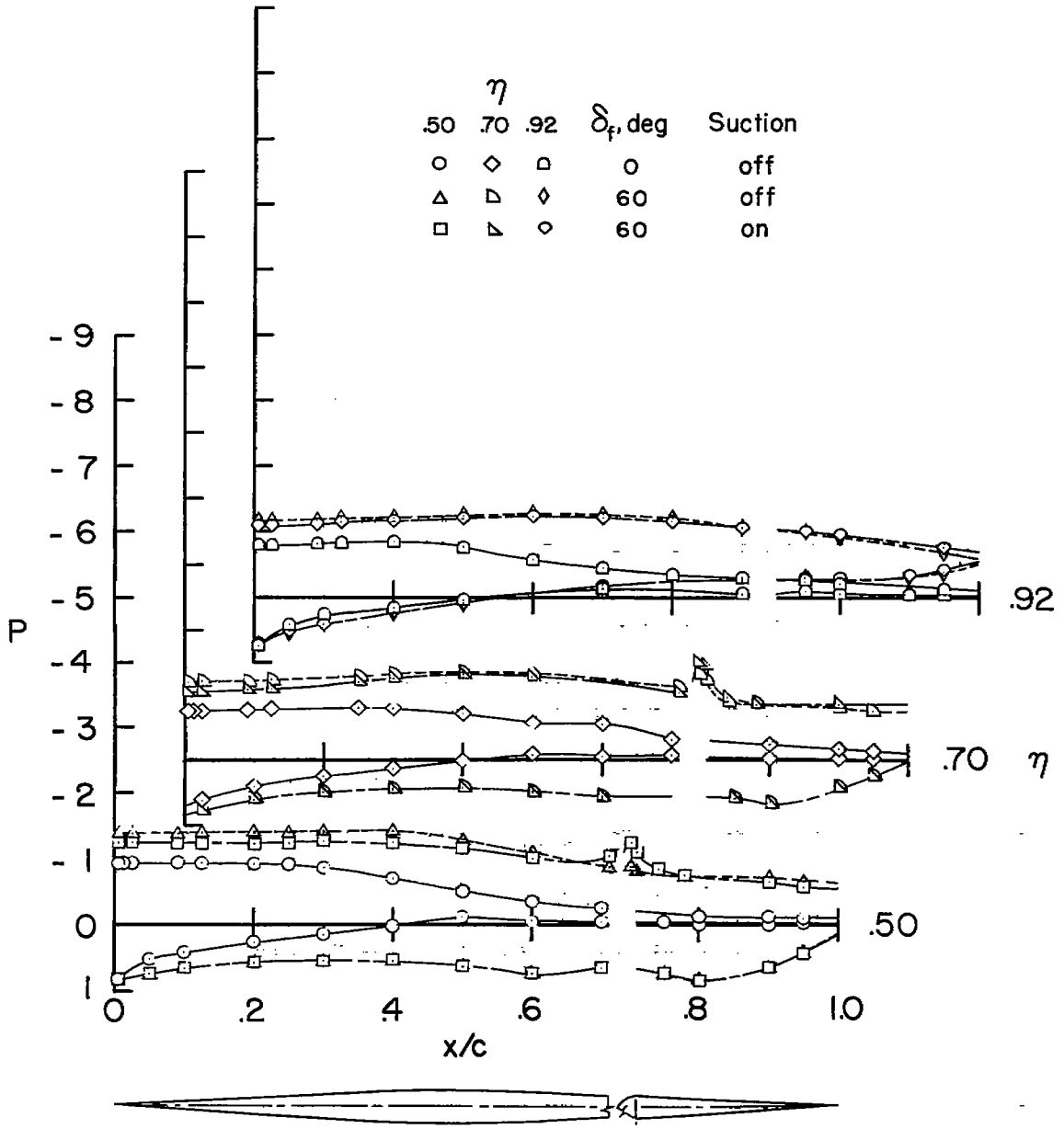

(c) $\alpha = 9.0^{\circ}$

Figure 7.- Concluded.

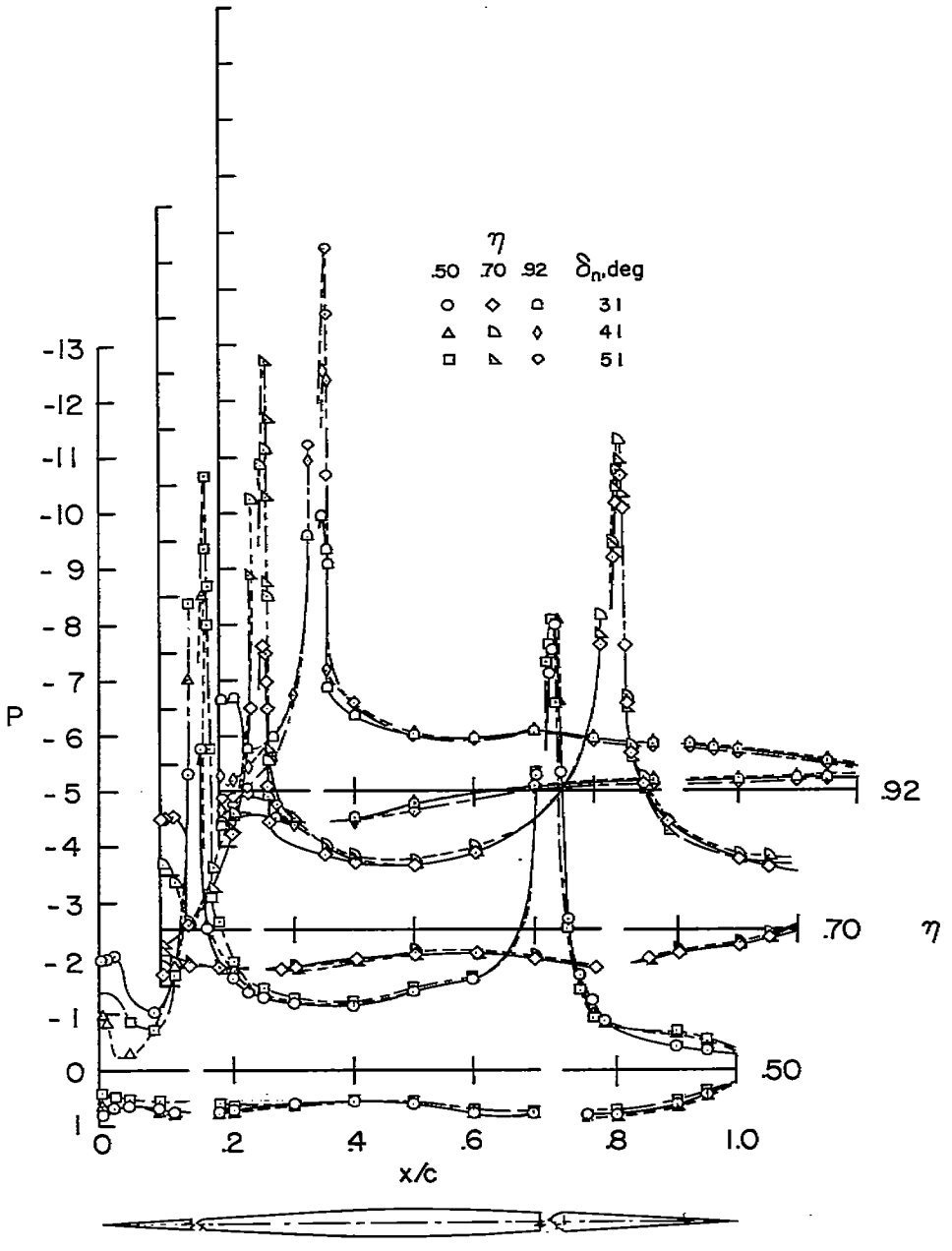

(a) $\alpha = 9.0^{\circ}$

Figure 8.- The effect of leading-edge flap deflection on the chordwise pressure distribution at high angles of attack; $\delta_f = 50^{\circ}$. For porous area and suction air-flow conditions, see table II. The x/c axis is broken at values of x/c corresponding to the flap hinge locations.

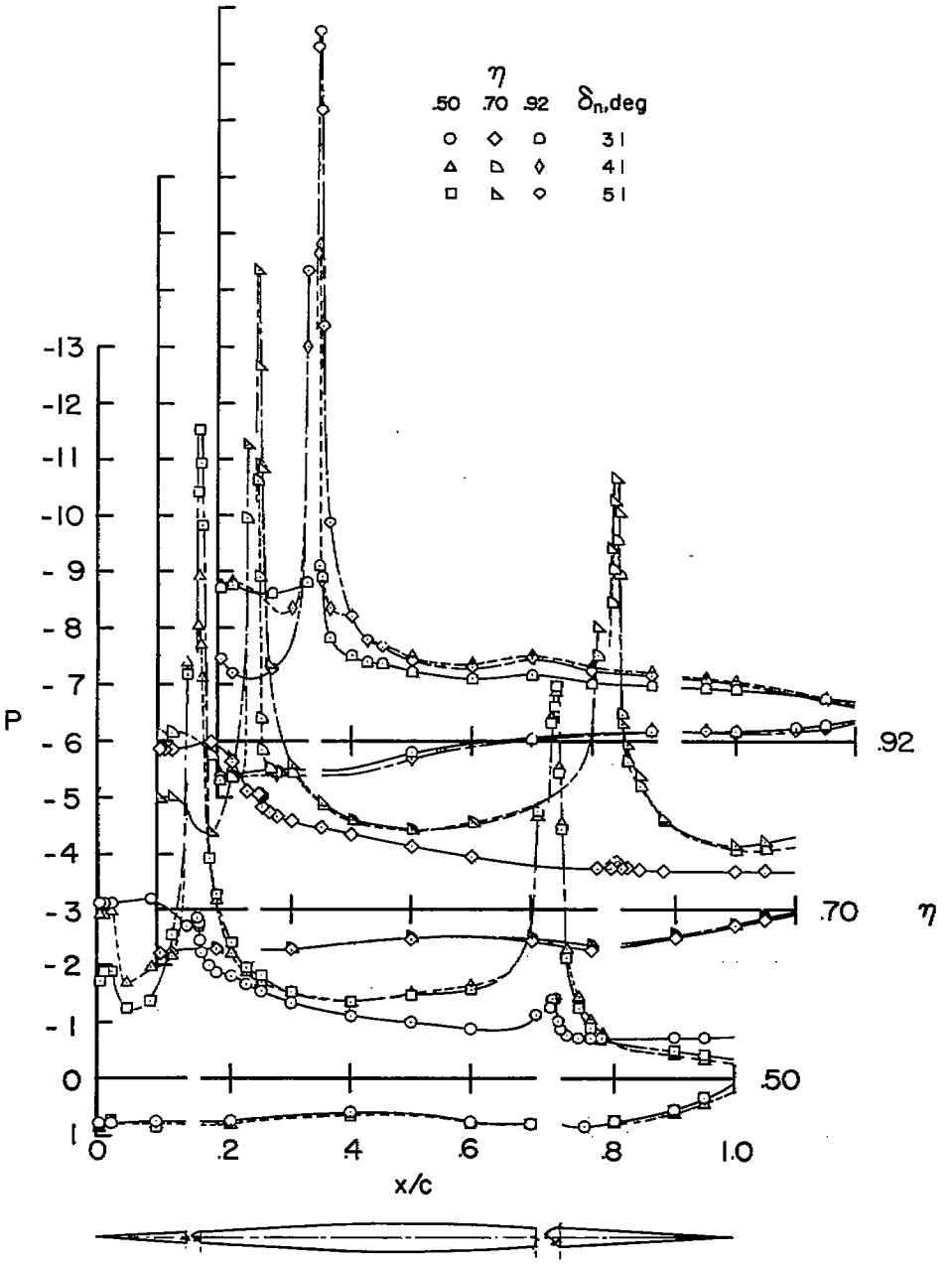

(b) $\alpha = 15.1^{\circ}$

Figure 8.- Continued.

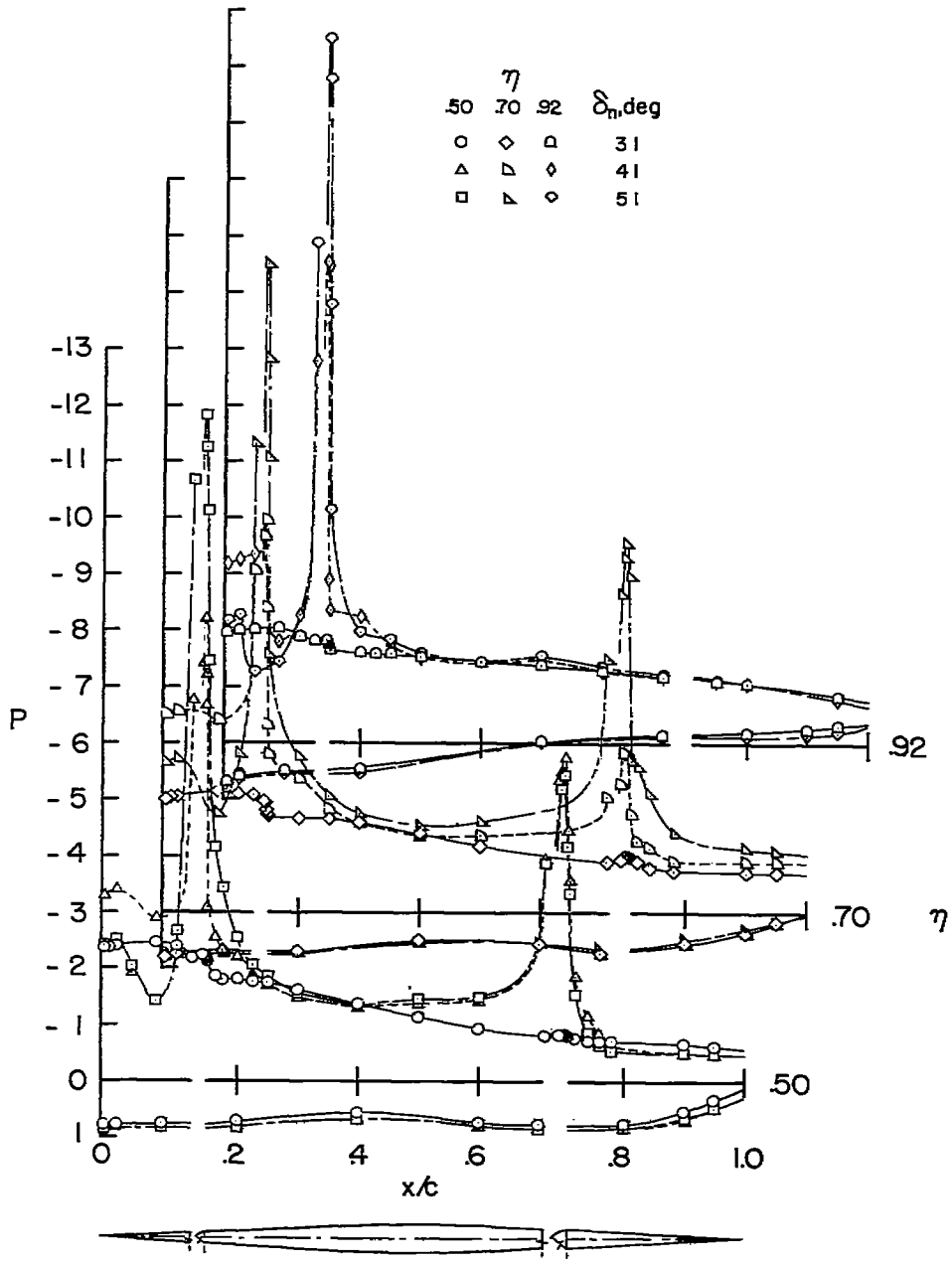

(c) $\alpha = 17.2^{\circ}$

Figure 8.- Concluded.

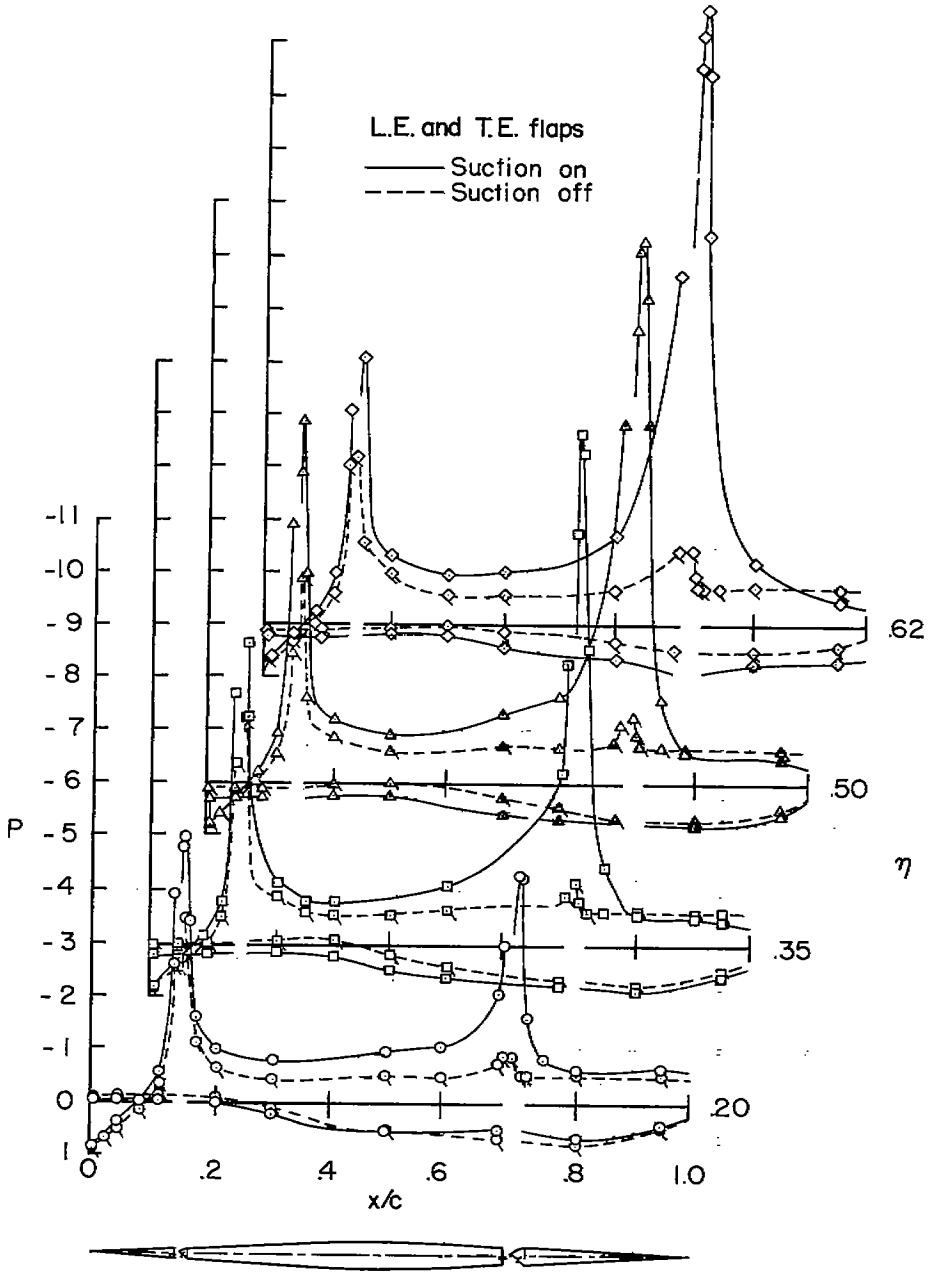

(a) $\alpha = 0.9^{\circ}$; $\eta = 0.20$ to 0.62

Figure 9.- The effect of porous area suction on the chordwise pressure distribution of the model with $\delta_n = 41^{\circ}$, $\delta_f = 60^{\circ}$. For porous area and suction air-flow conditions, see table II. The x/c axis is broken at values of x/c corresponding to the flap hinge locations.

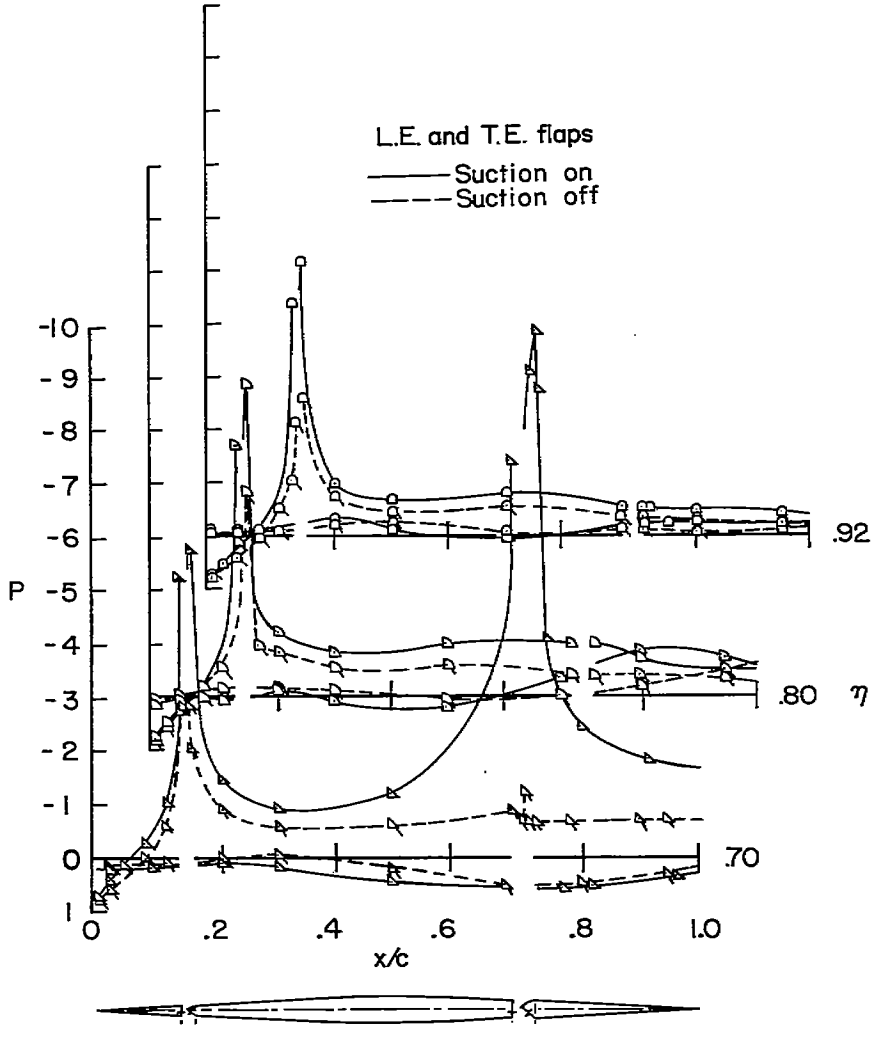

(b) $\alpha = 0.9^{\circ}$; $\eta = 0.70$ to 0.92

Figure 9.- Continued.

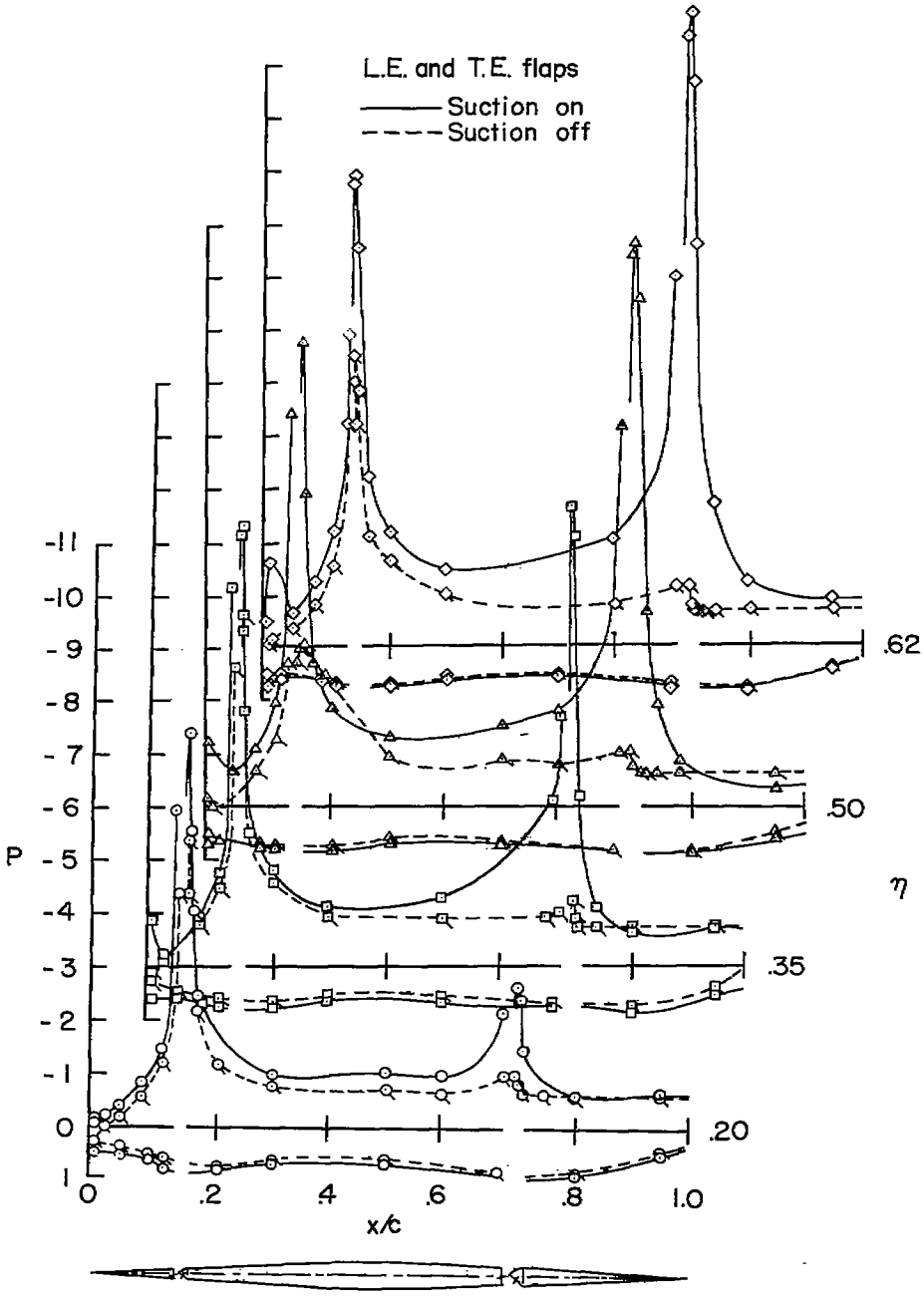

(c) $\alpha = 9.0^{\circ}$; $\eta = 0.20$ to 0.62

Figure 9.- Continued.

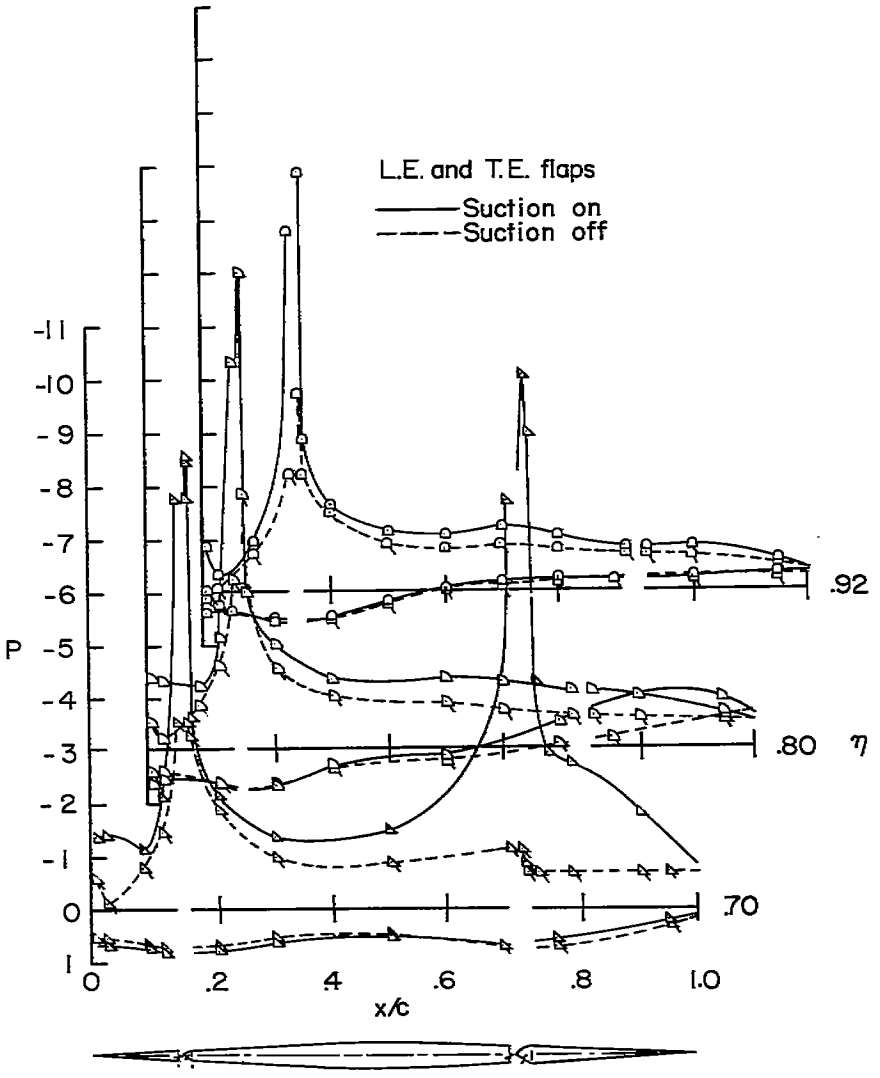

(d) $\alpha = 9.0^{\circ}$; $\eta = 0.70$ to 0.92

Figure 9.- Continued.

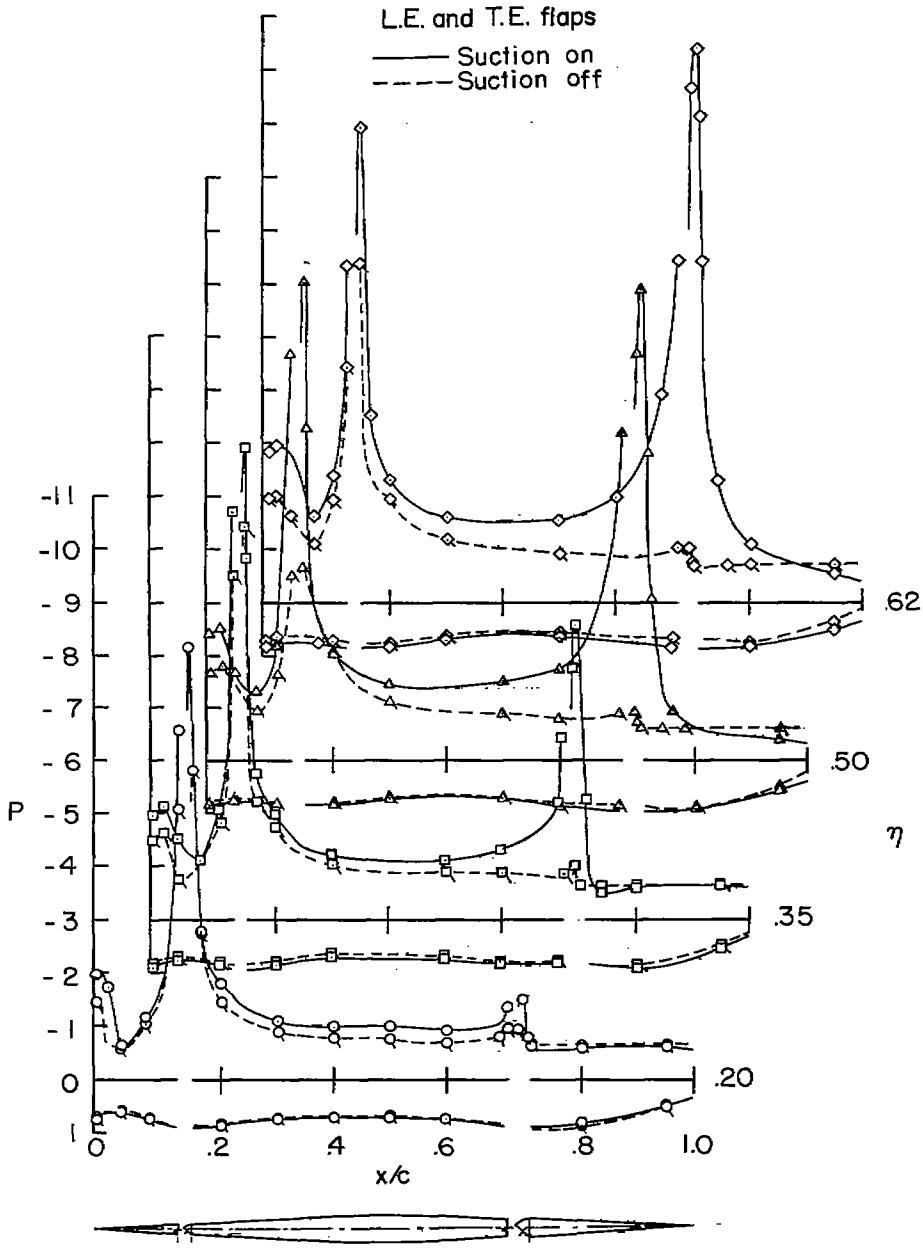

(e) $\alpha = 13.2^{\circ}$; $\eta = 0.20$ to 0.62

Figure 9.- Continued.

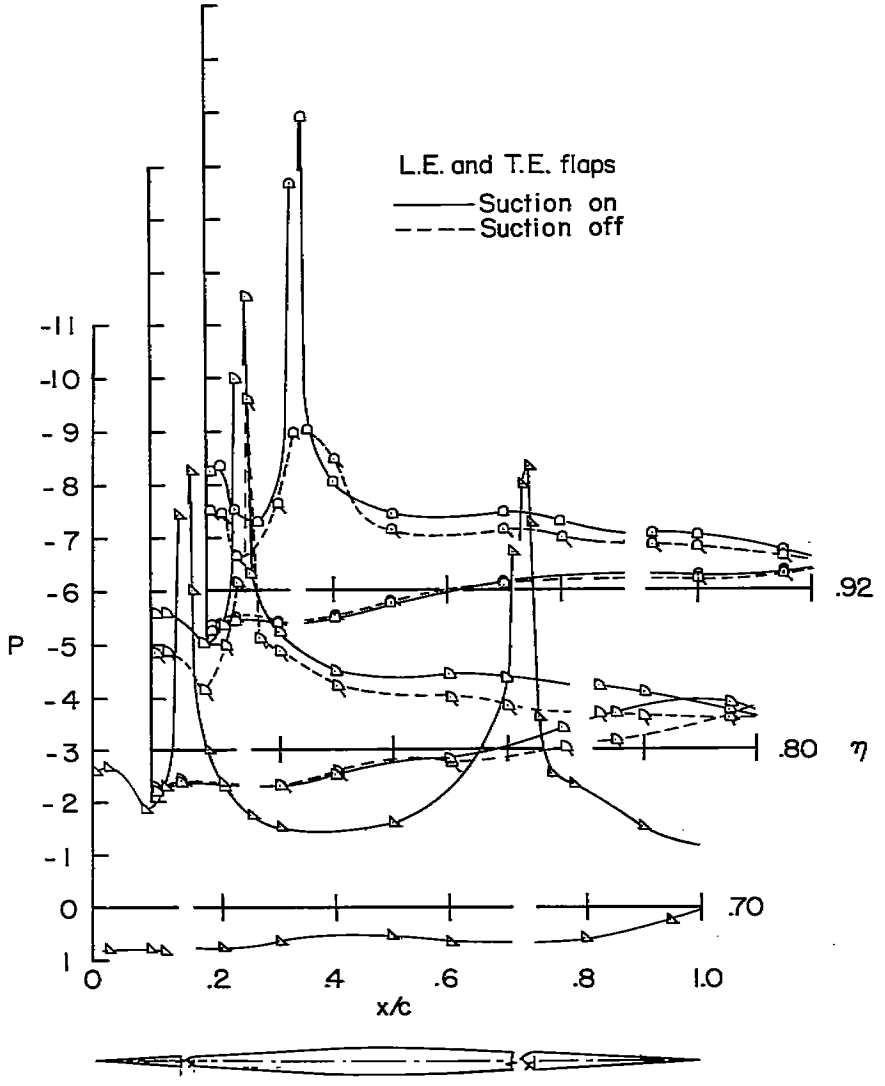

(f) $\alpha = 13.2^{\circ}$; $\eta = 0.70$ to 0.92

Figure 9.- Continued.

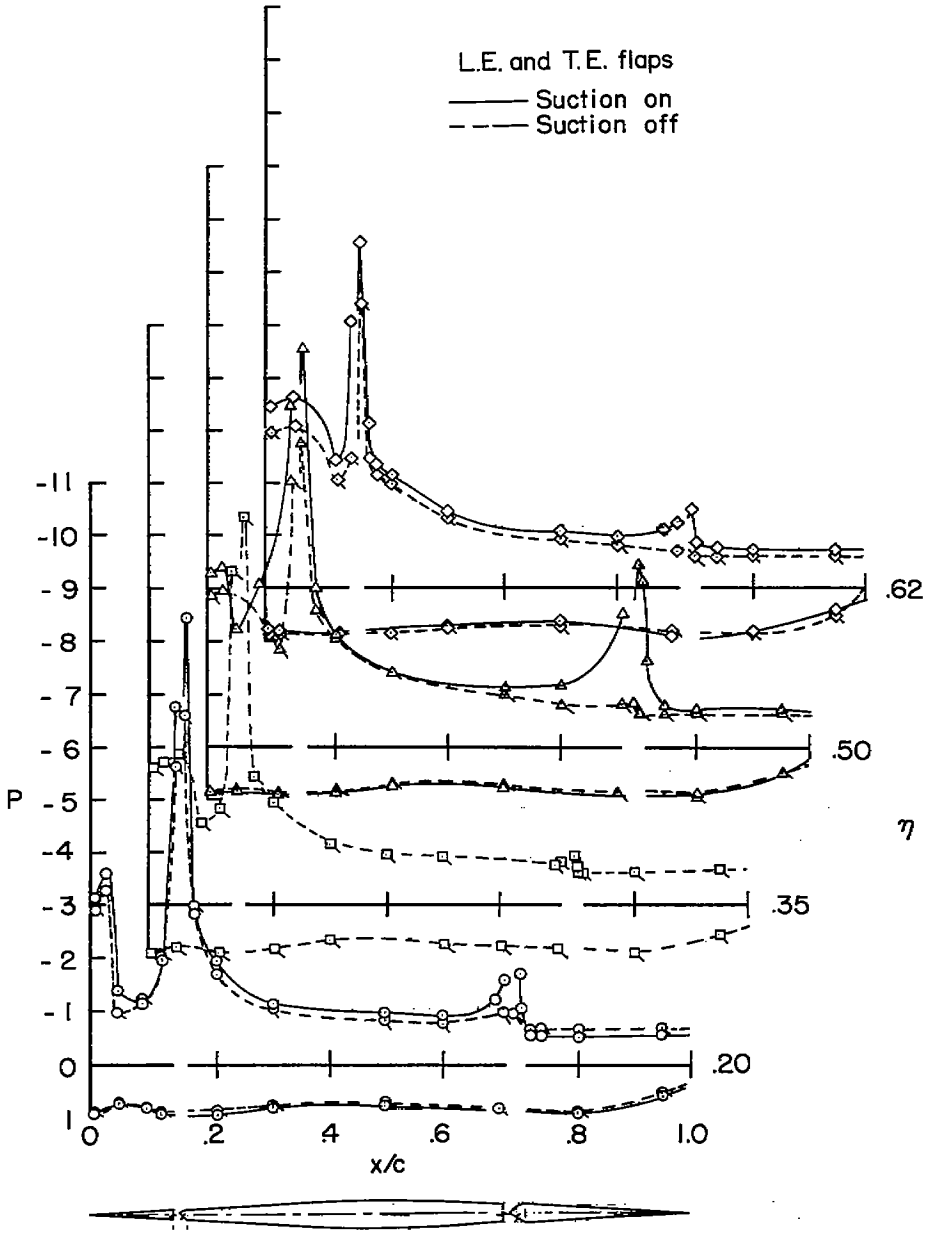

(g) $\alpha = 17.2^{\circ}$; $\eta = 0.20$ to 0.62

Figure 9.- Continued.

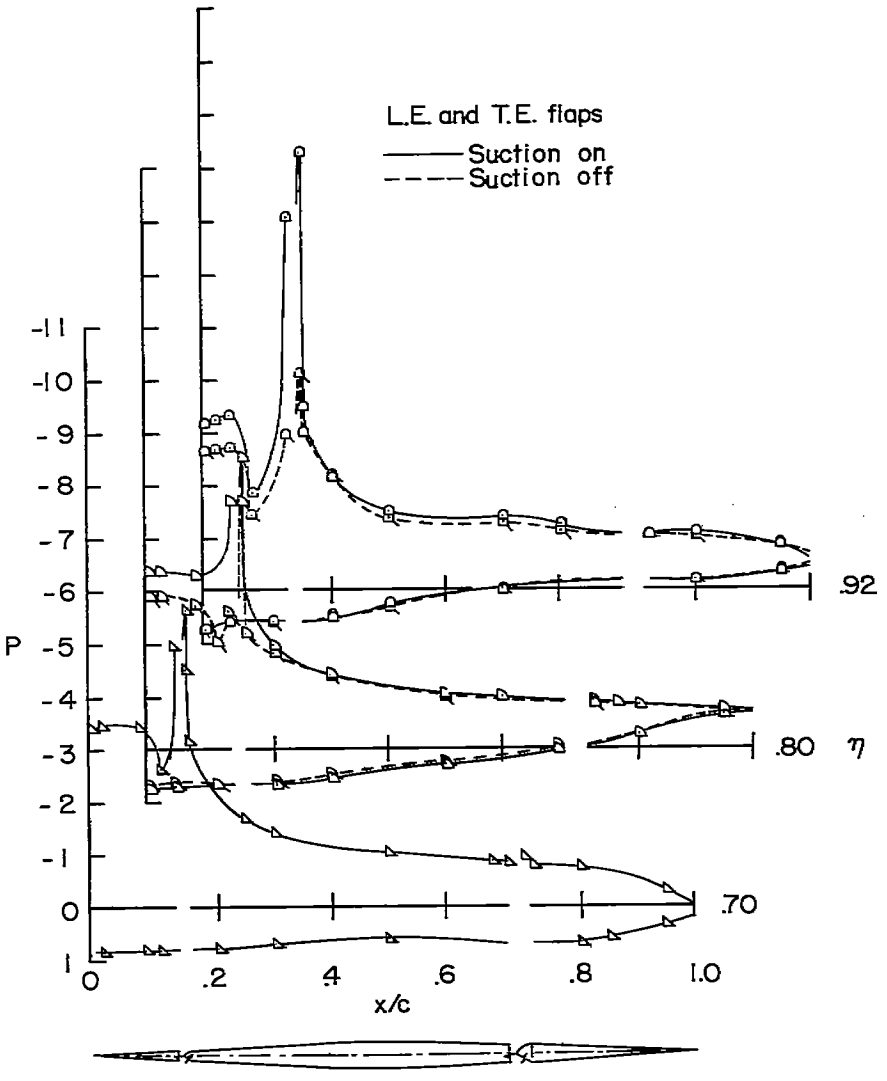

(h) $\alpha = 17.2^{\circ}$; $\eta = 0.70$ to 0.92

Figure 9.- Concluded.

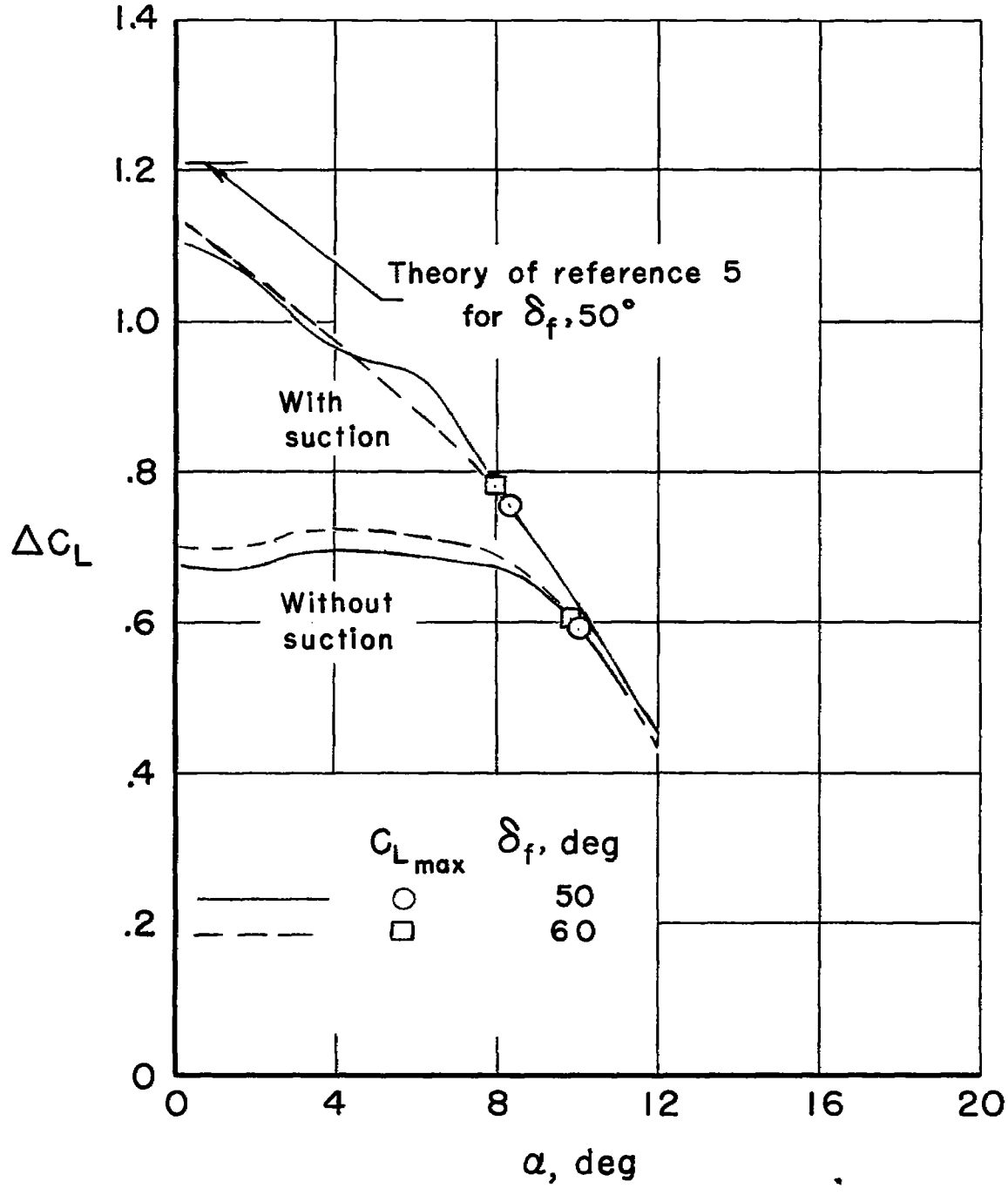

Figure 10.- The variation of the trailing-edge-flap lift increment with angle of attack of the model with the leading-edge flap undeflected.

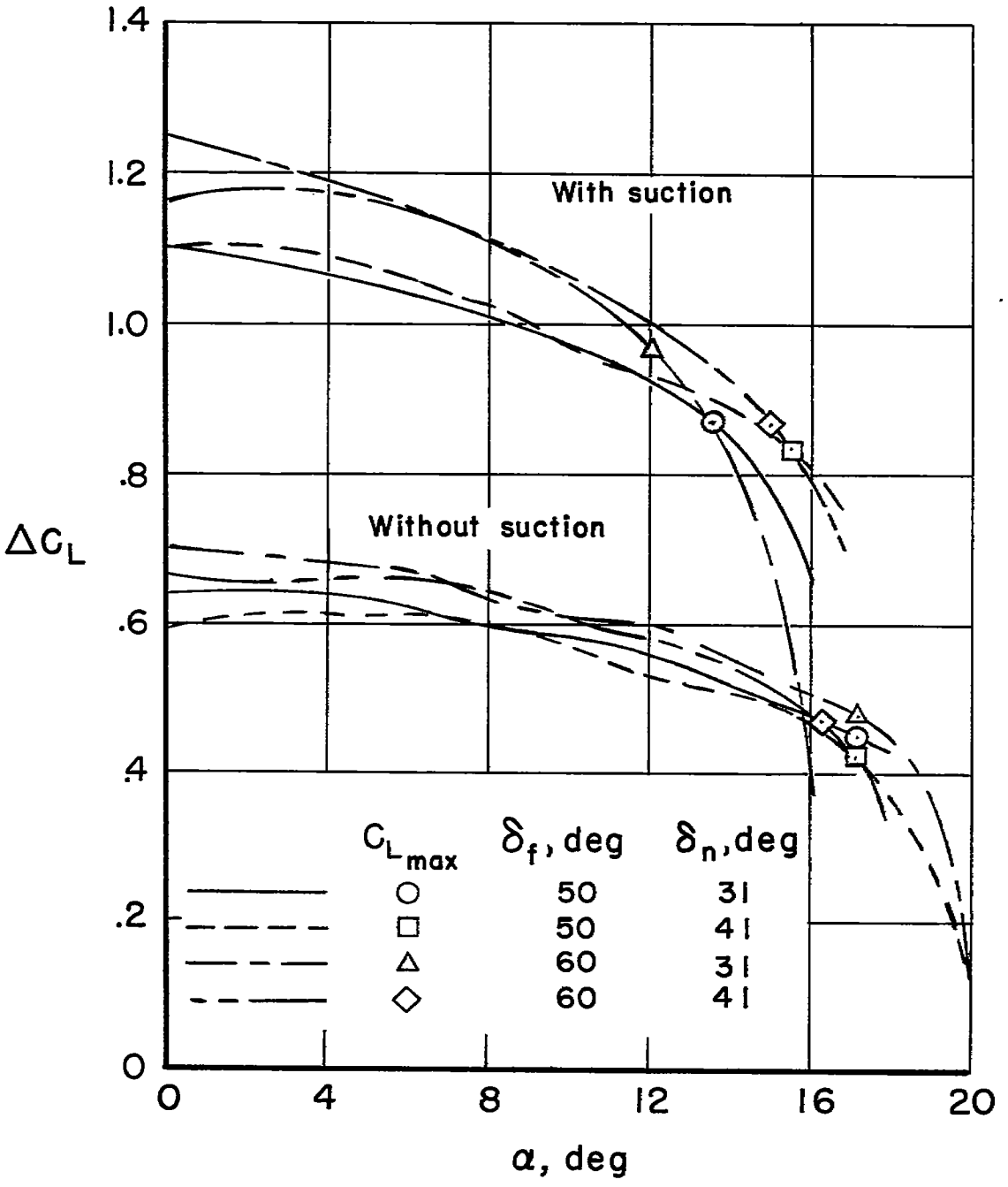

Figure 11.- The variation of trailing-edge-flap lift increment with angle of attack of the model with the leading-edge flaps deflected, either with or without suction on both leading and trailing-edge flaps.

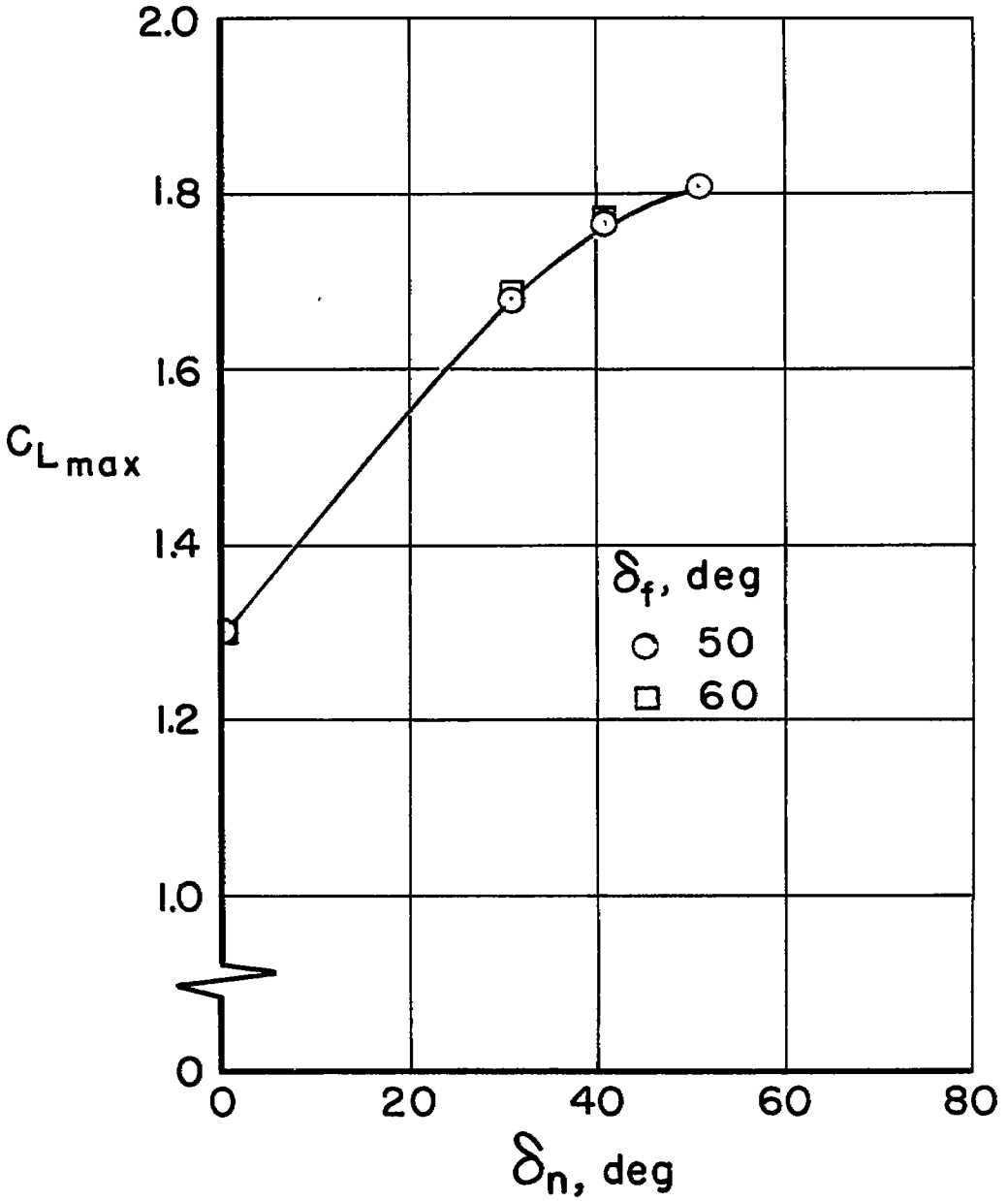

Figure 12.- The variation of the $C_{L_{max}}$ with nose flap deflection, δ_n; with suction on both leading- and trailing-edge flaps.

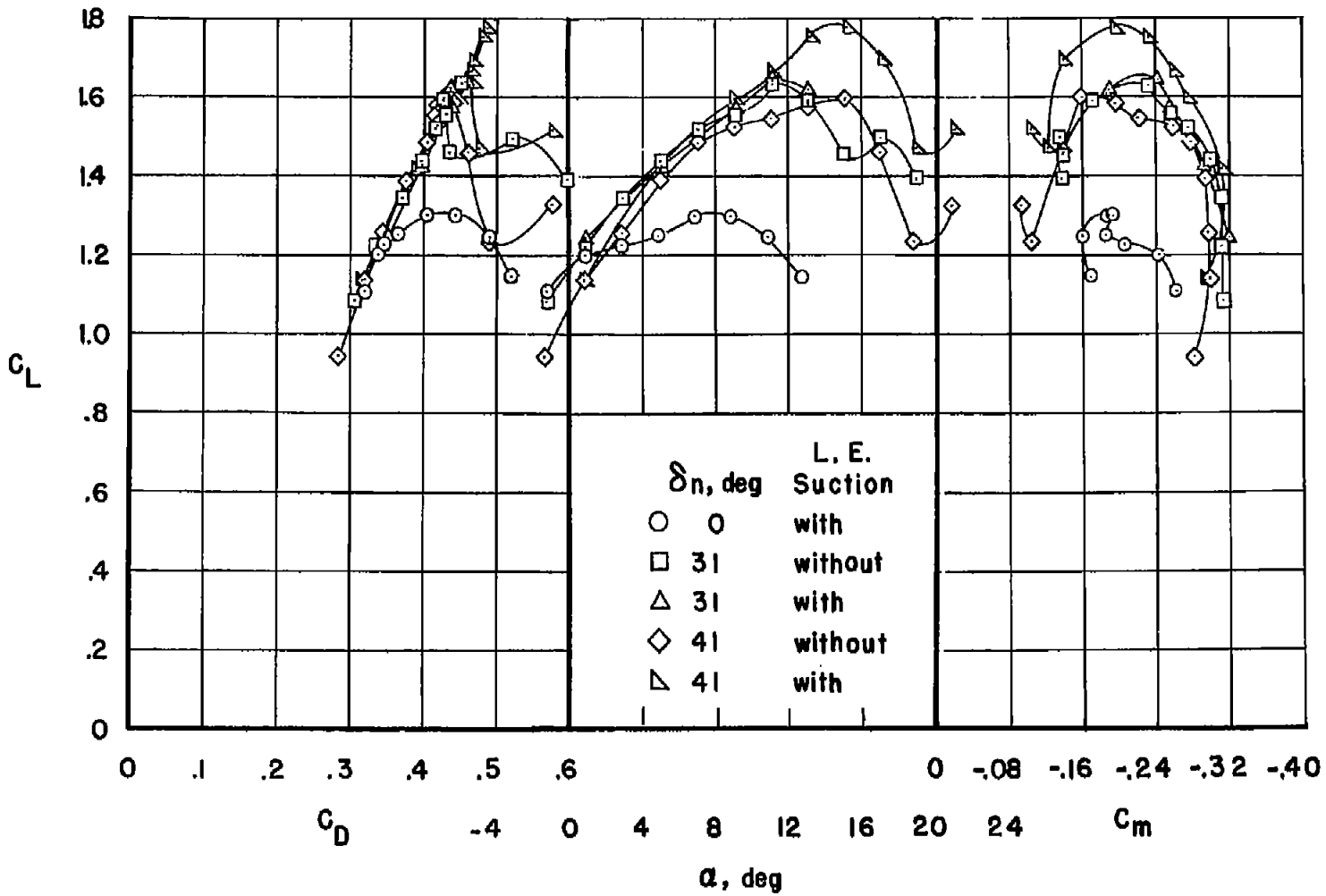

Figure 13.- The effect of applying area suction to the leading-edge flap on the force and moment characteristics of the model; $\delta_f = 60^\circ$, suction on. For porous area and suction air-flow conditions, see table II.

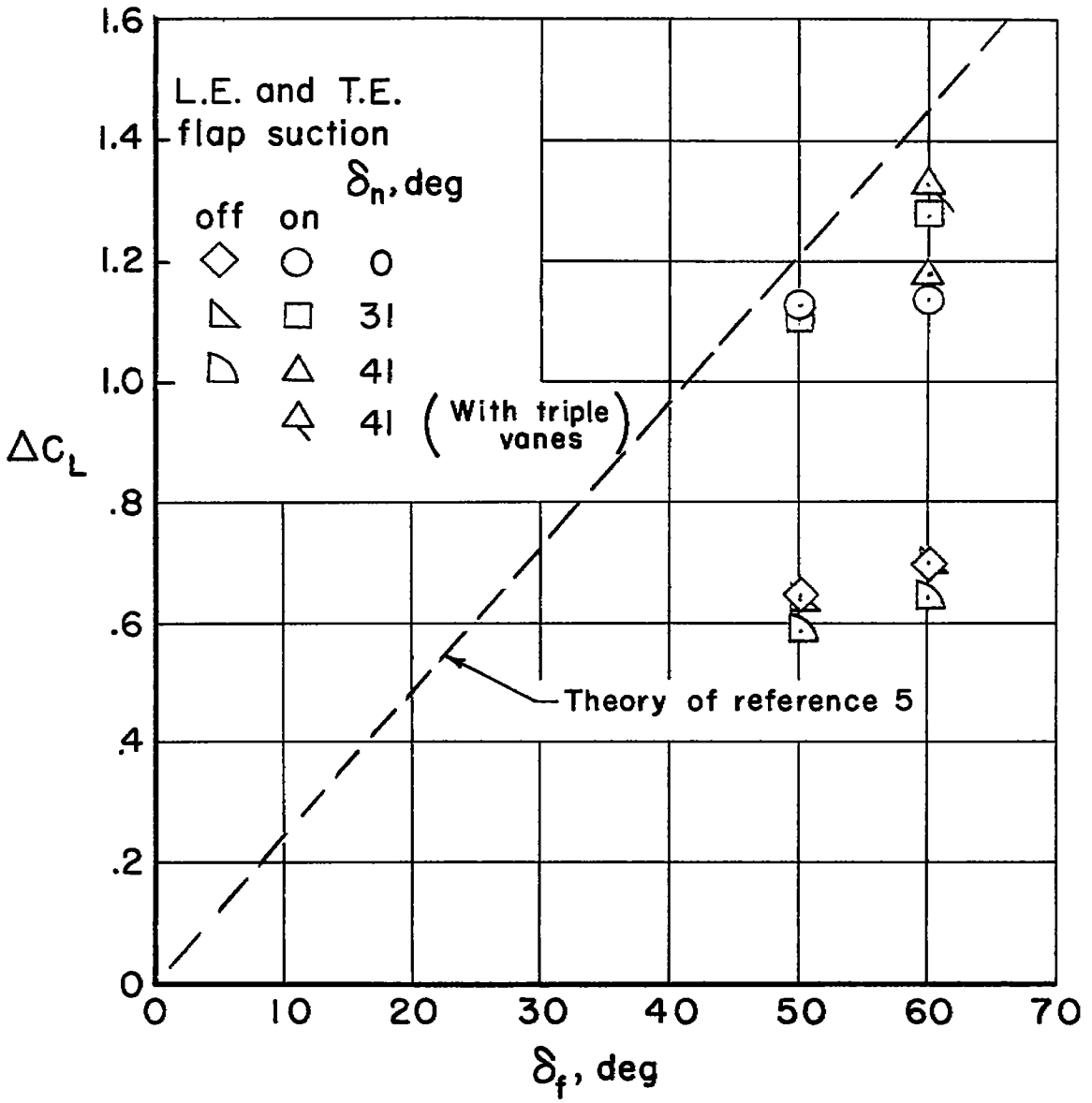

Figure 14.- The variations of trailing-edge-flap lift increment with flap deflection; $\alpha = 0^{\circ}$.

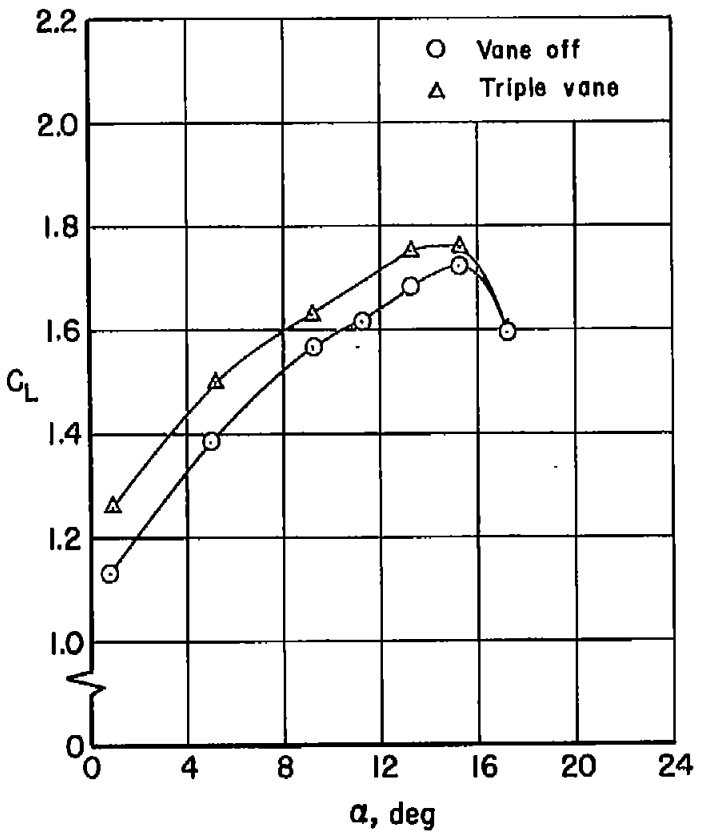

(a) C_L vs. α; C_Q = 0.0016

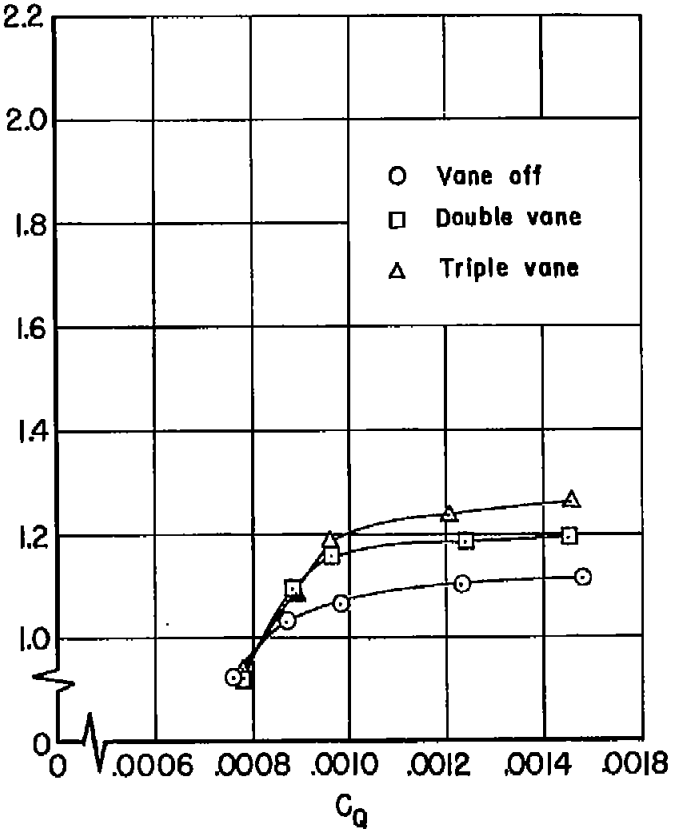

(b) C_L vs. C_Q; α = 0.8 deg

Figure 15.- The effect of turning vanes on the lift characteristics of the model with suction on the leading- and trailing-edge flaps for $\delta_n = 41^\circ$ and $\delta_f = 60^\circ$. For porous area and suction air-flow conditions, see table II.

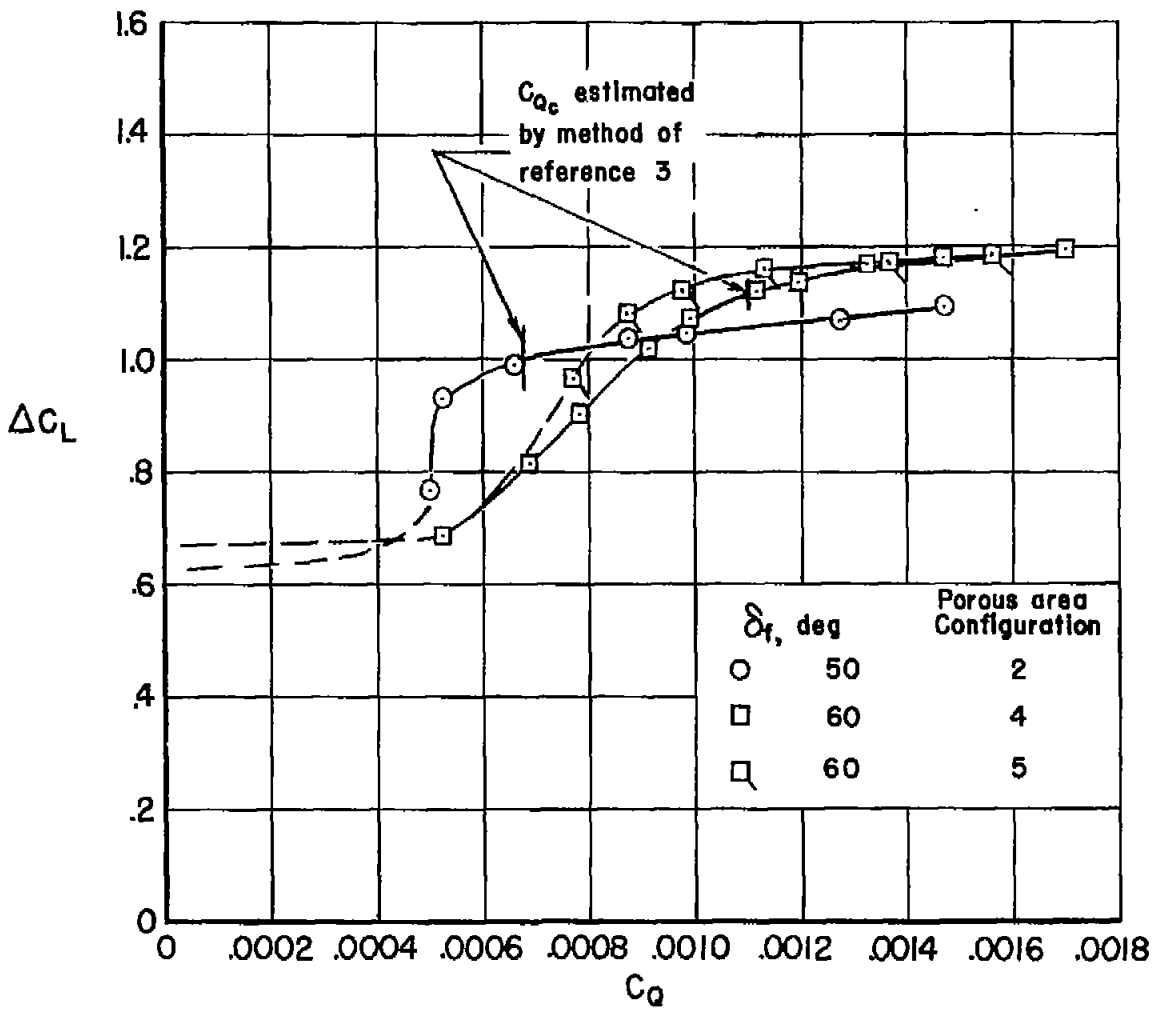

Figure 16.- The variation of flap lift increment with flow coefficient for two trailing-edge-flap deflections; $\alpha = 0.8^\circ$, $\delta_n = 41^\circ$ with suction on leading-edge flap.

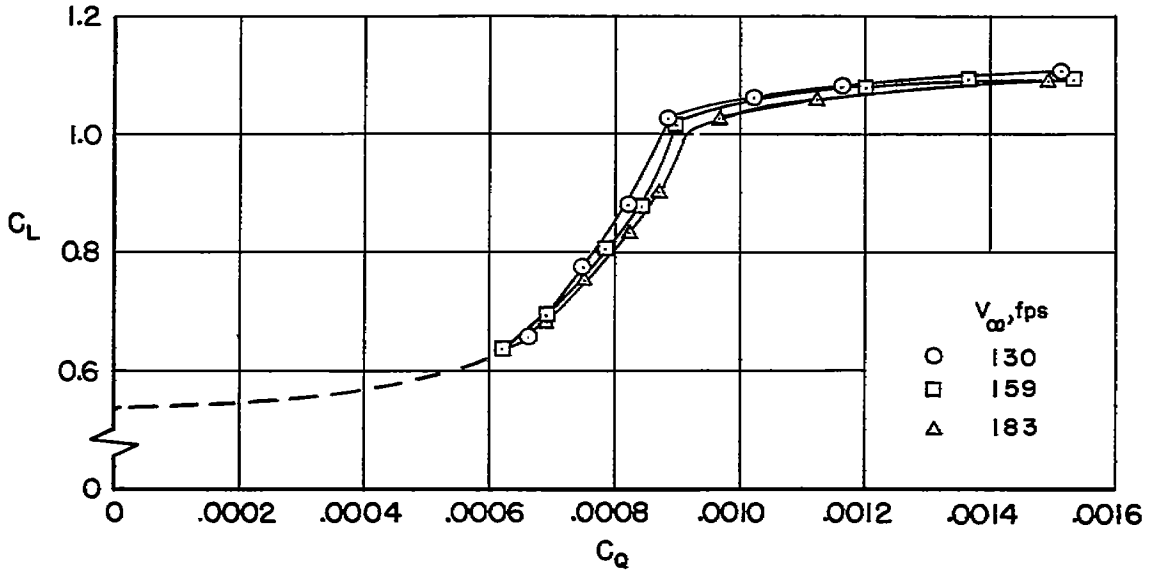

(a) C_L vs. C_Q

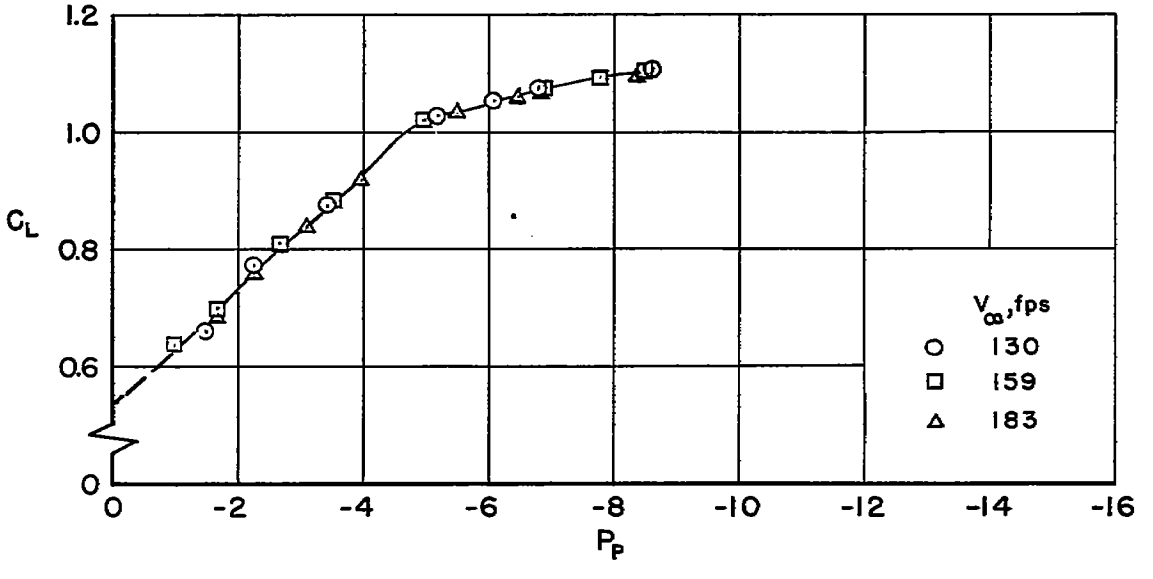

(b) C_L vs. P_P

Figure 17.- The effect of stream velocity on the suction flow requirements of the trailing-edge flap for $\delta_n = 41^\circ$ and $\delta_f = 50^\circ$; porous area configuration 1; $\alpha = 0.8^\circ$; suction on leading-edge-flap.

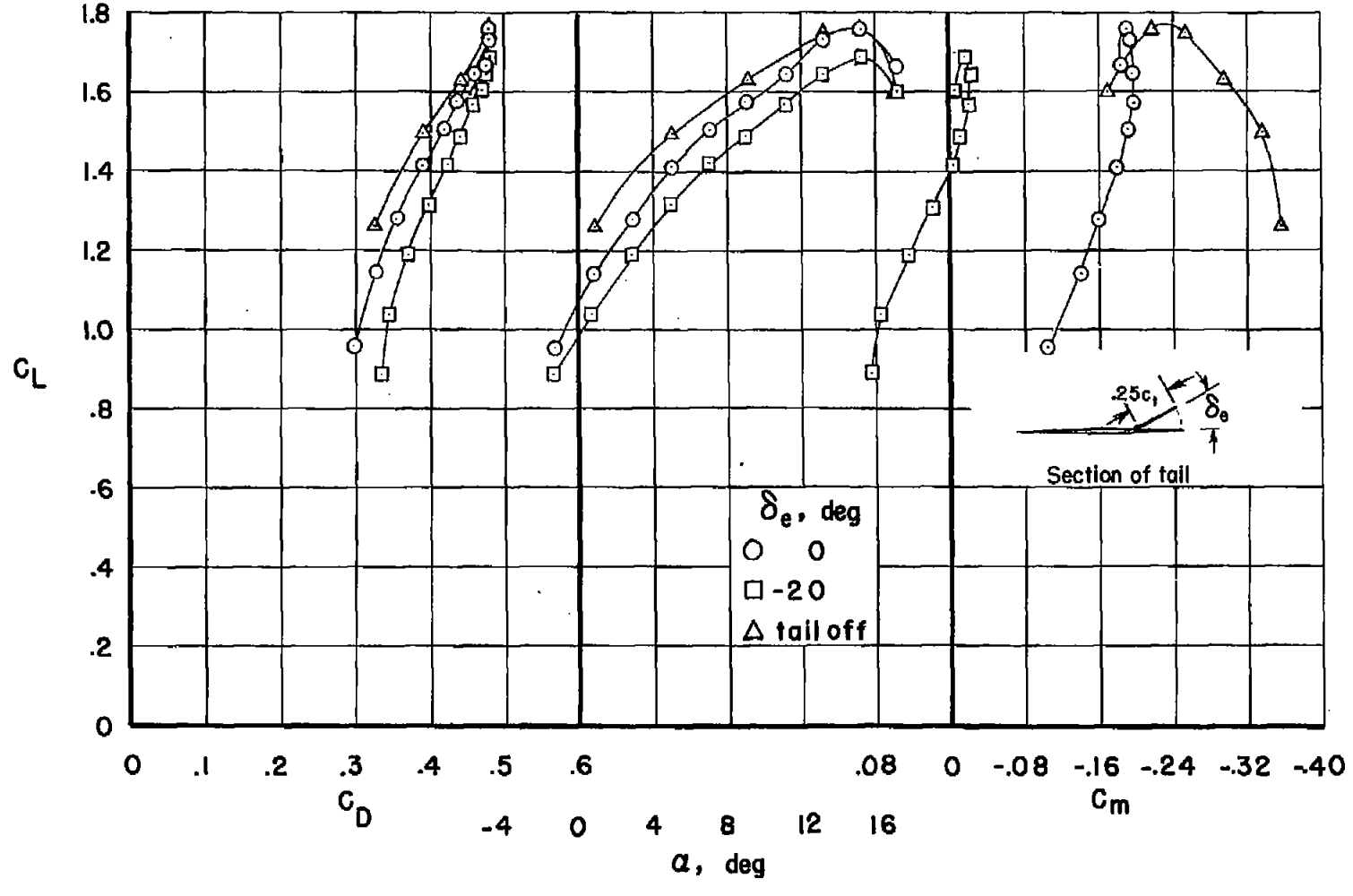

Figure 18.- Longitudinal characteristics of the model with an unswept horizontal tail; $\delta_n = 41^\circ$ and $\delta_f = 60^\circ$ with suction on both leading- and trailing-edge flaps; triple vanes installed. For porous area and suction air-flow conditions, see table II.